

# Review of CO<sub>2</sub> Laser Ablation Propulsion with Polyoxymethylene

John E. Sinko\* and Akihiro Sasoh†

\*Micro-Nano Global Center of Excellence, Graduate School of Engineering, Nagoya University, Furo-cho, Chikusa-ku, Nagoya, Aichi, Japan 464-8603

sinko@fuji.nuae.nagoya-u.ac.jp

†Department of Aerospace Engineering, Nagoya University, Furo-cho, Chikusa-ku, Nagoya, Aichi, Japan 464-8603 sasoh@nuae.nagoya-u.ac.jp

## Abstract

Polyoxymethylene (POM) has been widely studied as a promising laser propulsion propellant when paired to CO<sub>2</sub> laser radiation. POM is a good test case for studying ablation properties of polymer materials, and within limits, for study of general trends in laser ablation-induced impulse. Mechanisms such as vaporization, combustion, and plasma are evaluated and a description is made of the link between the fluence of the beam and the resulting temperature of the target. For characterization of propulsion parameters, almost all previous studies of POM considered limited ranges of ambient pressure and incident fluence. As a result, despite many studies, there is no general understanding of POM ablation that takes into account pressure, spot area, fluence, and effects from confinement and combustion. This paper reviews and synthesizes CO<sub>2</sub> laser ablation propulsion work using POM targets in order to make preliminary steps to address this deficiency. Previously published data is compared in terms of ablated mass as well as propulsion parameters such as momentum coupling coefficient ( $C_m$ ) and specific impulse ( $I_{sp}$ ), within a range of fluences from about  $1 \times 10^4$ - $5 \times 10^6$  J/m<sup>2</sup>, ambient pressures from  $10^{-2}$ - $10^5$  Pa, and laser spot areas from  $10^{-6}$ - $10^{-3}$  m<sup>2</sup>.

## NOMENCLATURE

Symbol	Unit	Description
$a$	[m <sup>2</sup> ]	Characteristic cross-sectional area of the laser beam spot
$A$	-	Atomic number
$c_p$	[J/kgK]	Heat capacity at constant pressure
$C_m$	[Ns/J]	Momentum coupling coefficient
$C_{opt}$	[Ns/J]	Maximum momentum coupling coefficient
$D$	[m <sup>2</sup> ]	Thermal diffusion coefficient
$E_a$	[J]	The fraction of deposited energy that does not drive propellant kinetic energy
$E_k$	[J]	Kinetic energy of exhaust
$E_L$	[J]	Total energy in one laser pulse
$f$	[Hz]	Pulse frequency of repetitive mode laser operation
$g$	[m/s <sup>2</sup> ]	Gravitational acceleration —erase subscript
$I$	[Ns]	Impulse
$I_{sp}$	[s]	Specific impulse
$m$	[kg]	Total ablated mass
$n_i$	[m <sup>-3</sup> ]	Number density of ionic species
$n_{mol}$	[m <sup>-3</sup> ]	Number density of molecular species
$n_o$	[m <sup>-3</sup> ]	Number density of neutral atomic species
$n_{ec}$	[m <sup>-3</sup> ]	Number density threshold for formation of critically dense plasma
$N$	-	Number of pulses
$t$	[s]	Time

$T$	[K]	Temperature
$T_m$	[K]	Melting point
$T_G$	[K]	Glass transition temperature
$T_b$	[K]	Boiling point
$z_a$	[m]	Threshold ablation depth
$v$	[m/s]	Particle speed
$\langle v \rangle$	[m/s]	Average particle speed
$v_{ex}$	[m/s]	Exhaust velocity
$Z$	-	Charge of ion
$a$	[m <sup>-1</sup> ]	Absorption coefficient
$\beta$	-	Ionization fraction
$\Delta H_f$		Latent heat of fusion
$\Delta H_g$		Heat of gasification
$\Delta T$	[K]	Change in temperature during laser heating
$\varepsilon$	-	Dielectric constant
$\eta_{ex}$	-	Efficiency of exhaust collimation
$\phi_A$	-	Absorptivity
$\phi_R$	-	Total reflectivity
$\phi_{Rdiff}$	-	Diffuse component of reflectivity
$\phi_{Rspec}$	-	Specular component of reflectivity
$\phi_T$	-	Transmissivity
$\Phi(z)$	[J/m <sup>2</sup> ]	Local fluence during one pulse as a function of depth from the ablator surface
$\Phi_a$	[J/m <sup>2</sup> ]	Threshold fluence for ablation
$\Phi(0)$	[J/m <sup>2</sup> ]	Effective fluence delivered just inside the ablator surface
$\Phi_L$	[J/m <sup>2</sup> ]	Fluence on ablator surface irradiated without plasma and reflection
$\Phi_{opt}$	[J/m <sup>2</sup> ]	Fluence at which the maximum momentum coupling coefficient is reached
$\Phi_p$	[J/m <sup>2</sup> ]	Threshold fluence for critical plasma formation
$\kappa$	[W/mK]	Thermal conductivity
$\lambda$	[m]	Wavelength
$\Lambda$	-	Non-dimensional fluence, normalized to the ablation threshold
$\Lambda_{opt}$	-	Non-dimensional fluence at which maximum $C_m$ is found
$\mu$	[kg/m <sup>2</sup> ]	Areal ablated mass density
$\Psi$	[W/m <sup>2</sup> ]	Irradiance of the laser pulse
$\rho$	[kg/m <sup>3</sup> ]	Density
$R$	[Wm]	Resistivity
$\sigma$	[Ns/m <sup>2</sup> ]	Areal impulse density
$\theta_d$	[rad]	Divergence half angle
$\theta_{ex}$	[rad]	Angle at which exhaust leaves the surface
$\tau$	[s]	Laser pulse length

## 1. INTRODUCTION

The CO<sub>2</sub> laser has become a valuable tool in material processing due to the easily accessible high output pulse energy (or average output power). It is not uncommon for industrial CO<sub>2</sub> lasers to output around 10 kW (describing either continuous wave or average power repetitive pulse systems). As early as 1972 [1], it was recognized that the output of CO<sub>2</sub> lasers could also be applied to laser propulsion. Early ablation efforts often used metal targets, and some efforts to use a kind of airbreathing propulsion mechanism were also made [2-4]. Neither metals nor air are, by themselves, particularly good absorbers of CO<sub>2</sub> laser radiation, as one class of propellants is strongly reflective, and the other transparent. The search for other propellants led to polymers, and specifically to polyoxymethylene.

Laboratory synthesis of polyoxymethylene (POM) was first reported in 1859 by Butlerow [5]. The debut of POM as a propellant matched to CO<sub>2</sub> lasers was probably made in the experiments at AVCO Everett and Physical Sciences, Inc. (PSI) [6,7] from 1987-1991. Further historical overview of this development effort was described by Kare [8]. POM has since been studied as a laser propulsion

propellant by groups all over the world [4,6-23]. POM exhibits excellent performance under CO<sub>2</sub> laser ablation in both atmospheric and vacuum conditions, compared to other polymers. For instance, maximum momentum coupling coefficient ( $C_m$ ) values on the order of 200 - 2000  $\mu\text{Ns/J}$  have been reported in the literature depending on experimental conditions [4,7,9-16,18-24]. Other common polymer candidates such as polymethylmethacrylate (PMMA) or polytetrafluoroethylene (PTFE) have much lower maxima, typically closer to 50-100  $\mu\text{Ns/J}$ . However, the properties of POM are not always advantageous; for instance, the maximum values for specific impulse ( $I_{sp}$ ) reported for most basic ablation experiments were only near 100-200 s [7,9-12,14,15,18,22,23]. Certainly, this range of  $I_{sp}$  values is low from the standpoint of desirable propellant properties for laser propulsion, which generally seeks to present a high- $I_{sp}$  alternative to chemical systems limited to around  $I_{sp} \approx 450$  s. However, confinement (*e.g.*, using nozzles [23]) can increase  $I_{sp}$  above 1000 s.

Laser propulsion applications for POM are envisioned from atmospheric [6-8,9-12,14-19,21-24] to outer space [13,20,21] environments. There are many phenomena which can influence the propulsion performance over the broad parameter spaces covered by the various possible laser systems, operating environments, and vehicle geometries. Our motivation for assembling this review is primarily to clarify the basic physics of POM ablation and impulse generation. However, we also aim to elucidate the ways in which the improved understanding of ablation physics can be applied to practical engineering applications. Many literature studies that address CO<sub>2</sub> laser ablation of POM have been assembled in order to draw such general conclusions and identify gaps in the current understanding. It is our hope that future works can efficiently address the dark areas highlighted by this review.

## 2. MATERIAL CHARACTERISTICS

POM is widely used in laser ablation propulsion experiments. An immediate question is, why? What makes POM a good propellant choice? The answer is complex, and requires a careful consideration of POM in terms of its optical and thermal properties, as these characteristics strongly influence its behavior under ablation. However, as will be discussed later, material properties are not the only considerations.

### 2.1 Chemical formula and basic properties

POM is polyoxymethylene, also called polyacetal, by which is meant  $[\text{CH}_2\text{O}]_n$ , with the basic structure illustrated in Figure 1a. Commercial POM is often stabilized, for instance, in the manner illustrated in Figure 1b.

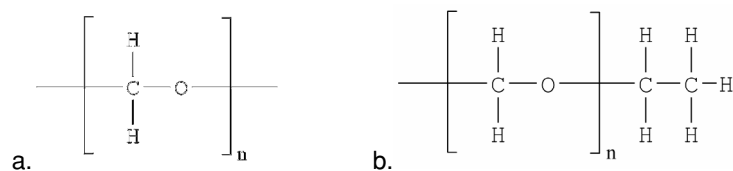


Figure 1. Chemical structure of (a) POM homopolymer and (b) one of many possible forms of stabilized POM

The implications of this sort of stabilization are discussed in more detail later in this paper. POM degrades to formaldehyde (CH<sub>2</sub>O) in response to heating, with a molecular weight of about 30 g/mol, and an average molecular weight of about 7.5 g/mol when fully atomized.

The first choice confronting researchers seeking to study ablation of POM is what sort of POM is best for study. At present, homopolymer POM is sold under several trade names. Two of the most common include Delrin® (Dupont), Sustarin H® (Röchling), and Tecaform AD® (Ensinger High Performance Plastics). Copolymers include Acetron® (Quadrant Engineering Plastic Products), Celcon® and Hostaform® (Ticona Engineering Polymers, a subsidiary of Celanese Corporation), Iupital® (Mitsubishi Engineering Plastics Corp.), Kepital® (Korea Engineering Plastics Co.), Duracon® and Tepcon® (Polyplastics Co., Ltd.), Pomalux® (Westlake Plastics Co.), Sustarin C® (Röchling Engineering Plastics), Ensital® and Tecaform AH® (Ensinger High Performance Plastics), Ultraform® (BASF Corp.), and Unital® (Nytel Plastics). This list is not intended to represent any endorsement for the particular companies or polymer varieties by the authors, but merely to illustrate the large number of possible sources for POM targets.

The most evident distinction in the above list is between homopolymer and copolymer varieties. At high temperatures, homopolymer POM is known to degrade by a rapid ‘unzipping’ mechanism, regenerating the formaldehyde monomer. This has obvious unpleasant consequences for many high-temperature applications. Stabilized POM copolymers typically include ethylene groups interspersed in the polymer chain to inhibit this degradation pathway. It is possible that homopolymer POM may exhibit better performance than copolymer POM for laser ablation propulsion applications, since a more rapid, explosive reaction should be created if the laser ablation degradation mechanism is uninhibited. However, it is also possible that cleavage of the polymer at random positions in the chain during laser energy deposition could largely bypass the stabilized positions. In that case, little difference would be observed between homopolymer and copolymer varieties. Further study is necessary to determine whether stabilization significantly impedes laser ablation in this context. Among other considerations, the copolymer seems likely to exhibit better long-term stability in the space environment, so for space applications it seems likely that ethylene-stabilized varieties are preferable to the homopolymer.

In addition, the copolymer varieties may be expected to differ in chemical and physical characteristics. Typical C-C bond energies are around 350 kJ/mol, as compared to C-O bond energies of  $\approx 360$  J/mol, so despite impeding the aforementioned radical unzipping reaction, copolymers may actually be slightly easier to ablate via bond-breaking reactions than the homopolymer. Van der Waal forces and conformations of the polymer chains may also be slightly different between homopolymer and copolymer varieties. The net effect on ablation properties such as the boiling point and density is not completely clear. One may expect that the absorption spectrum will be different, due to the differences in bonding characteristics. So far, to the authors’ knowledge, there has been no comprehensive study of POM copolymer spectra. Some efforts at creating custom POM varieties (*e.g.*, by doping or mixing) to enhance ablation performance will also be discussed later in this paper.

## 1.2 Thermal Properties

As mentioned above, an understanding of the thermal properties of POM is essential for understanding the ablation process. Details will be discussed in subsequent sections. Representative thermal data for POM is given in Tables 1-5. It may be noted that POM is generally not special with regard to its thermal properties, compared to other polymers.

**Table 1. Thermal Conductivity ( $\kappa$ )**

Researcher	$\kappa$ [W/(m K)]	Reference
Haji-Sheikh, <i>et al.</i>	$0.38 - (T \times 4.52 \times 10^{-4})$ ( <i>e.g.</i> , $\kappa_T \approx 0.24$ W/(m K) at $T = 300$ K)	[25]
LaHoucine and Khellaf	0.235, 0.240	[26]
Madhusoodanan, <i>et al.</i>	0.285, 0.268	[27]
Representative value used in this paper	0.25 W/(m K)	

**Table 2. Thermal Diffusivity ( $D$ )**

Researcher	$D$ [m <sup>2</sup> /s]	Reference
Haji-Sheikh, <i>et al.</i>	$D = 4.35 \cdot 10^{-7} - (T \times 7.80 \times 10^{-10})$ ( <i>e.g.</i> , $D_T \approx 2.0 \times 10^{-7}$ for $T=300$ K)	[25]
Holve	$3.5\text{-}5.2 \cdot 10^{-8}$	[28]
Madhusoodanan, <i>et al.</i>	$1.37 \times 10^{-7}, 1.29 \times 10^{-7}$	[27]
Representative value used in this paper	$1 \times 10^{-7}$ m <sup>2</sup> /s	

**Table 3. Heat Capacity ( $c_p$ )**

Researcher	$c_p$ [J/(kg K)]	Reference
Line fit to Dainton, <i>et al.</i>	$c_p \approx 4.84 T$ ( <i>e.g.</i> , $C_p \approx 1450$ J/(kg K) at $T = 300$ K)	[29]
Weast	1500	[30]
Representative value used in this paper	1500 J/(kg K)	

**Table 4. Latent Heat of Fusion ( $\Delta H_f$ )**

Researcher	$H_f$ [J/kg]	Reference
Iguchi	$3.15 \times 10^5$	[31]
Inoue	$2.23 \times 10^5$ (crystal)	[32]
Inoue, <i>et al.</i>	$1.74 \times 10^5$	[33]
Starkweather and Boyd	$2.46 \times 10^5$ (crystal)	[34]
	$1.79 \times 10^5$	
Starkweather and Jones	$2.48 \times 10^5$ (crystal)	[35]
	$3.89 \times 10^5$	
Wilski	$1.82$ - $1.92 \times 10^5$ (annealed sample)	[36]
	$3.17$ - $3.35 \times 10^5$ (crystal)	
Representative value used in this paper	$2 \times 10^5$ J/kg	

**Table 5. Heat of Gasification ( $\Delta H_g$ )**

Researcher	$H_g$ [J/kg]	Reference
Lyon	$2.4 \times 10^6$	[37]
Stoliarov and Walters	$(3.37 \pm 0.32) \times 10^6$	[38]
Representative value used in this paper	$3 \times 10^6$ J/kg	

Most of the thermal properties are dependent on the crystallinity of the sample; in fact, the dependence on crystallinity is well established [39].

### 1.3 Thermal Degradation

Since CO<sub>2</sub> laser ablation produces rapid heating at the material surface, it will be instructive to consider the response of POM during exposure to high temperatures. In the context of this review, we will begin by examining the behavior of solid POM at room temperature, and work our way to the vapor phase. Of course, as noted by Anisimov [40], at any finite temperature, every material also has a nonzero vapor pressure, so some insignificant degree of material removal occurs even at room temperature.

Sukhanova, *et al.* [41] studied a variety of POM samples and gave a range of glass transition temperatures ( $T_G$ ) around 300-400 K and melting points ( $T_m$ ) from 410-450 K. Jaffe and Wunderlich [42] studied homopolymer POM and reported  $T_m \approx 450$ -460 K. As is typical for polymers, at sufficient temperatures beyond the melting point, a range of degradation phenomena are observed in heated POM, rather than a clear vaporization point. For instance, in a PVT diagram published by Starkweather, *et al.* [35], an upper-limit melting temperature of about 450-460 K is given in vacuum, and an approximate threshold for degradation phenomena at around 490 K. The melting point was

observed to increase significantly at high pressure. Abu-Isa, *et al.* [43] reported a characteristic threshold temperature for degradation phenomena around 525 K, described as proceeding by rapid, thermally-driven, free-radical degradation processes. Kern and Cherdron [44,45] also showed that the POM degradation mechanism was thermally driven. Moreover, they showed that degradation proceeds from chain ends in an unzipping process that quickly liberates monomer (*i.e.*, formaldehyde: CH<sub>2</sub>O). Above 430 K in an oxygen-bearing atmosphere such as air, an auto-oxidative process was also observed to contribute to degradation. Duan, *et al.* [46] used thermogravimetric Fourier Transform Infrared (TG-FTIR) spectroscopy over a range of temperatures from 270-670 K and confirmed that POM degradation proceeded from chain ends such as (...-O-CH<sub>2</sub>OH), liberating formaldehyde monomer (CH<sub>2</sub>O) units until a more stable end-group such as ethylene (...-CH<sub>2</sub>-CH<sub>3</sub>OH) terminated the chain. The Duan, *et al.* study then divided POM degradation into four stages, based on the temperature of the material:

1. Release of water and some production of formaldehyde (~270-420 K)
2. Production of formaldehyde (~420-500 K)
3. Production of formaldehyde and carbon monoxide (500-570 K)
4. Production of formaldehyde, carbon monoxide, and methanol (>570 K)

The initial release of water at relatively low temperature has important implications for the ablation of POM by CO<sub>2</sub> laser radiation, since water is a strong absorber at 10.6 mm wavelength (see, *e.g.*, Reference 47). This effect will be discussed in more detail later.

Above about 570-670 K, random chain scission was found to dominate the degradation process. Under this mechanism, fragmentation of the polymer occurs at random points in the chain, so that the POM material is rapidly vaporized into a distribution of smaller fragments; however, even at this stage, the distribution was still found to be dominated by formaldehyde units. It may be mentioned here that exposure of POM to environmental ionizing radiation should result in limited degradation effects of a similar nature. Of no small importance is the suggestion in Reference 46 that at temperatures up to about 670 K, the exhaust gases initially produced by POM ablation are relatively transparent to CO<sub>2</sub> laser radiation (excluding water vapor).

In an oxygen atmosphere, the degradation products (especially formaldehyde and methanol) are expected to combust at sufficient temperatures. Thorough research by Ageichik, *et al.* [21] studied combustion of POM in an air atmosphere. The fluences used correspond roughly to the temperatures studied by Duan, *et al.* [46]. Combustion of POM was also studied by Beckel [48,49], who addressed time to ignition during continuous wave (cw) CO<sub>2</sub> laser irradiation of POM targets. To the knowledge of the authors, the distribution of ablation products of POM for  $T < 1000$  K has not been studied in the literature in any detail.

Andre [50] studied the high-temperature chemistry of several polymers (including POM) from about 1,270-10,270 K, under the assumption of local thermal equilibrium (LTE) and ambient atmospheric pressure (see Figures 2-5). For ablation phenomena, this range of temperatures begins in the realm of vaporization and extends into the plasma regime. Of course, the degree to which laser ablation meets any equilibrium conditions is limited; nevertheless, the paper provides critical data about the dissociation of POM into various species at high temperatures. Between about 1,300-2,300 K, the equilibrium gas composition is dominated by a mixture of H<sub>2</sub>O, CH<sub>2</sub>, CO<sub>2</sub>, CO, H<sub>2</sub>, and atomic hydrogen. Above about 2,300 K, the concentration of CH<sub>2</sub>, H<sub>2</sub>O, and CO<sub>2</sub> simultaneously and sharply declines. H<sub>2</sub> follows in a slow decline above about 4,300 K, as the concentration of atomic C and O become important within the same temperature range. Even distorted by non-equilibrium conditions, these effects should influence the combustion chemistry, and will also affect energy deposition and performance for laser ablation propulsion.

The electron number density increases sharply between about 4,300-10,300 K. This transition region links the vaporization regime to the plasma regime. The influence of carbon monoxide molecule remains strong until about 7,300 K, where it follows H<sub>2</sub> in slow decline. The influence of atomic hydrogen continues to be important even at the upper temperature limit of the study. The number densities of H<sup>+</sup> and O<sup>+</sup> were still increasing at 10,300 K, but were significantly below those for C<sup>+</sup>. The increase in C<sup>+</sup> over 4,300-10,300 K closely paralleled the increase in electron number density. It is clear from these results that the gaseous composition of POM contains many species, and is a strong function of the surface temperature. The ionization ratio begins to increase at about 4,300 K, and increases sharply thereafter; however, the gas is still far from being fully ionized at 10,300 K. Therefore, it is likely that the threshold fluence for significant plasma attenuation generally corresponds

to a temperature in excess of 10,300 K. From a propulsion standpoint, the composition is also important as applied to the ablatants, because the ratio of species can affect the velocity distribution of the exhaust.

Tanaka, *et al.* [51] recently published a study concerning C,H,O-type exhaust gas mixtures at temperatures from 300-30,000 K, well into the plasma regime. Part of the analysis used a 50%/50% CO<sub>2</sub>/H<sub>2</sub> gaseous mixture. This is not quite the same as POM exhaust (*i.e.*, the analysis effectively uses CH<sub>2</sub>O<sub>2</sub> instead of CH<sub>2</sub>O); however, ablation of POM in an oxygen-bearing atmosphere (*e.g.*, air) could produce a similar result. The results are consistent with the aforementioned studies, and indicate that H<sub>2</sub>, CO<sub>2</sub>, H<sub>2</sub>O, and CH<sub>4</sub> species should be important between about 300-3,000 K. From 3,000-13,000 K, it was found that atomic H, C, O, and CO make up the majority of the species, generally supporting Andre's treatment. Above about 13,000 K, beyond the range of the Andre study, the ionic species dominate, and the plasma regime has been reached. The Tanaka, *et al.* dataset also advances the understanding because it addresses ambient pressures from 0.1 to 10 MPa; specifically, the behavior at elevated pressures is important for atmospheric laser ablation of POM. The Tanaka, *et al.* study also reports many other thermodynamical quantities which would be of use to researchers in this topic.

A selection of the most important species in the Andre study are shown in Figures 2-5 (in general, this selection includes those with number densities exceeding 10<sup>18</sup> m<sup>-3</sup>). The species are presented in order of relevance with increasing temperature. First, molecular species are presented in Figure 2, then atomic species in Figure 3, and finally ionic species in Figure 4.

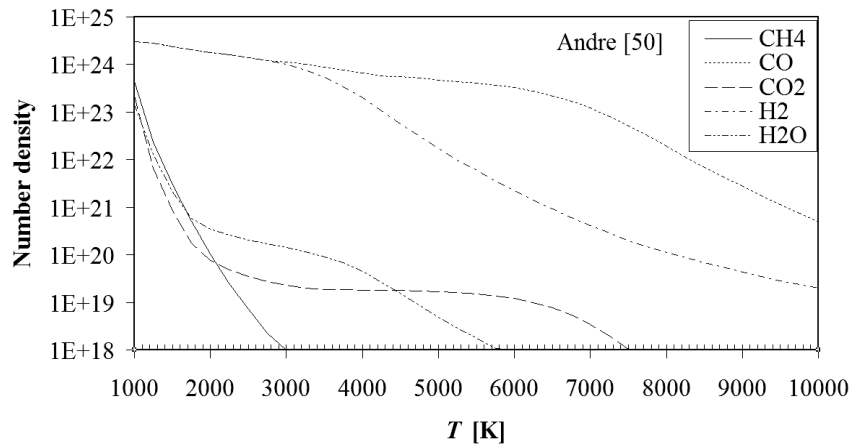


Figure 2.  $n_{mol}[T]$ ,  $10^5$  Pa, LTE conditions [50]

\*Material reproduced with permission, originally published as part of Figure 4, P. Andre, "Composition and thermodynamic properties of ablated vapours of PMMA, PA6-6, PETP, POM and PE", J. Phys. D: Appl. Phys., 29(7), IOP Publishing, Ltd., 1996, p. 1968.

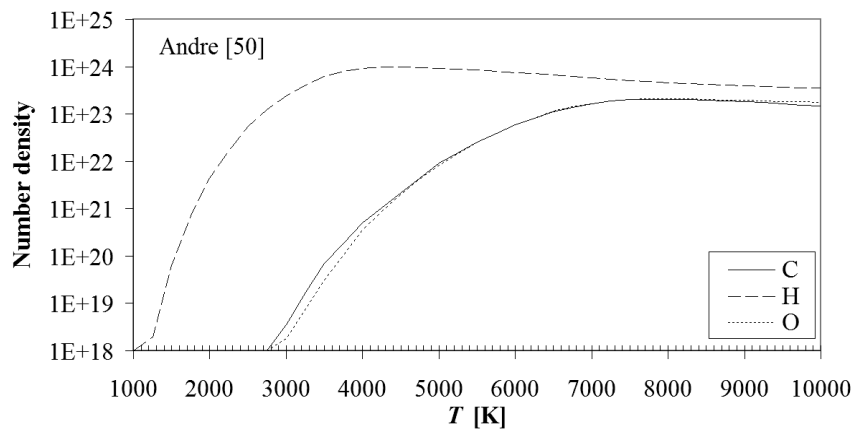


Figure 3.  $n_o[T]$ ,  $10^5$  Pa, LTE conditions [50]

\*Material reproduced with permission, originally published as part of Figure 4, P. Andre, "Composition and thermodynamic properties of ablated vapours of PMMA, PA6-6, PETP, POM and PE", J. Phys. D: Appl. Phys., 29(7), IOP Publishing, Ltd., 1996, p. 1968.

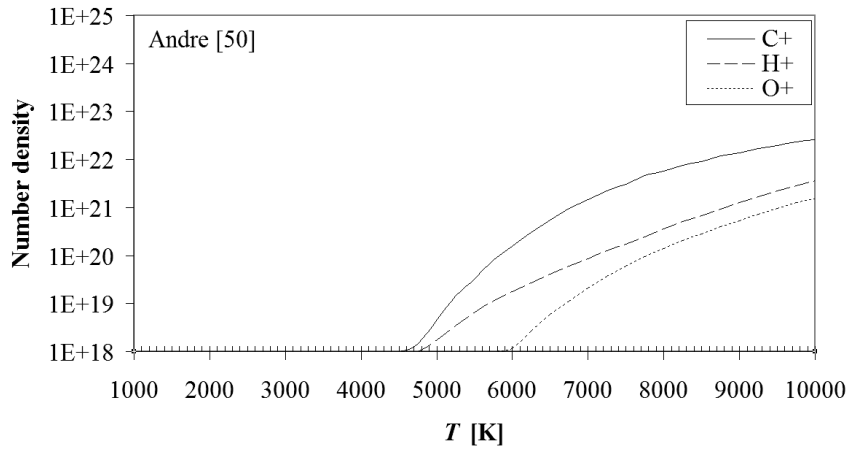


Figure 4.  $n_i(T)$ ,  $10^5$  Pa, LTE conditions [50]

\*Material reproduced with permission, originally published as part of Figure 4, P. Andre, "Composition and thermodynamic properties of ablated vapours of PMMA, PA6-6, PETP, POM and PE", J. Phys. D: Appl. Phys., 29(7), IOP Publishing, Ltd., 1996, p. 1968.

In the above plots, one may note that by far, the dominant molecular gas species are H<sub>2</sub> and CO. The atomization of gases takes place from about 2000-5000 K, and ionized species probably become dominant between about 10,000-20,000 K, above the upper range of the Andre study. The transition to the plasma regime is largely governed by the ionization fraction ( $\beta$ ):

$$\beta = \frac{n_e}{n_e + n_i + n_o + n_{mol}} \quad (1)$$

At typical plasma temperatures, we may generally neglect  $n_{mol}$ . Because of the intensity of the laser pulse, multiple ionization can occur. In both the Andre and Tanaka data, multiple ionization was accounted for, but multiply ionized species did not make up a significant part of the plasma within the temperatures studied (300-30000 K). At elevated temperatures where  $\beta \rightarrow 1$ , absorption of the laser radiation proceeds by inverse bremsstrahlung (IB). Plasma attenuation behavior (plasma shielding) appears at the threshold temperature for avalanche photoionization, at which the plasma quickly approaches 100% absorption after a critical electron density ( $n_{ec}$ ) is exceeded. From a physics standpoint, the threshold behavior is very different at high and low pressures, but in either case relates to energy dissipation from the plasma volume. At high pressure, energy dissipation is dominated by collisions with the surrounding neutral gas, and at low pressure, dissipation is dominated by electron diffusion out of the plasma volume [52]. Phipps previously provided a formula for calculating  $n_{ec}$  [53]:

$$n_{ec} \approx 1.115 \times 10^{15} / \lambda^2 m^{-3}, \quad (1)$$

where  $\lambda$  [m] is the ablating laser wavelength. For radiation at 10.6  $\mu$ m, this density is predicted to be  $n_{ec} \approx 1 \times 10^{25} m^{-3}$ .

The Andre data for  $\beta$ , plotted as ionization fraction, is shown in Figure 5. However, at the upper range temperature (10,000 K), the ionization fraction is still far from 100%.

It is important to note that the data in Figure 5 was generated for conditions of thermodynamic equilibrium, when in fact laser ablation is typically well-removed from such conditions. The pressure associated with a typical laser ablation event can range much higher than  $10^5$  Pa, which influences the ionization ratio. Nevertheless, the work is important in establishing probable important species in POM exhaust at a given temperature, and for estimating the critical temperature threshold for plasma formation. Absorption in plasma once  $n_{ec}$  is reached will result in attenuation of the laser pulse. The attenuation may be expressed using the plasma absorptivity  $\phi_A$  as a reduction factor of  $(1-\phi_A)$  multiplied with the fluence. In fact, since  $\phi_A$  varies with temperature, the absorption is itself dependent on the fluence. Some implications of this fact will be discussed in the next few sections. It may be

reiterated that the results of Duan, *et al.* [46] suggest that absorption by exhaust gases generated during ablation of POM does not play a significant role in attenuation unless critically dense plasma is formed.

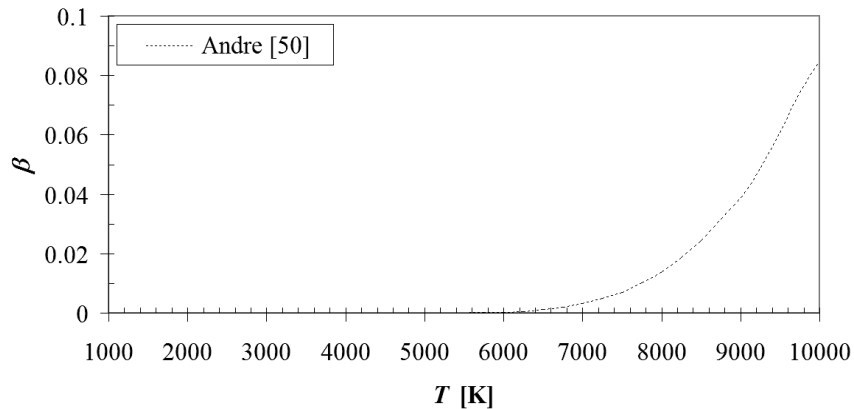


Figure 5.  $\beta(T)$  for POM gas mix, at a pressure of  $\approx 10^5$  Pa [50]

\*Material reproduced with permission, originally published as part of Figure 4, P. Andre, "Composition and thermodynamic properties of ablated vapours of PMMA, PA6-6, PETP, POM and PE", J. Phys. D: Appl. Phys., 29(7), IOP Publishing, Ltd., 1996, p. 1968.

### 1.4 Reflectivity and Transmissivity

Having provided a description of the effects of heating POM, it is also important to understand how the laser energy is able to enter the material to effect heating and vaporization. One may expect that the energy actually passing into the material will be reduced by various external phenomena (*e.g.*, plasma absorption above the surface, as mentioned above). One major reduction stems from reflection losses, which are mediated by the reflectivity  $\phi_R$  of the target surface, in the form of the transmission factor  $(1-\phi_R)$ . In fact, the issue is more complex, since the reflectivity is composed of both specular ( $\phi_{Rspec}$ ) and diffuse ( $\phi_{Rdiff}$ ) components; *i.e.*,  $\phi_R = \phi_{Rspec} + \phi_{Rdiff}$ . The specular reflectivity at a surface depends on the real part of the refractive index ( $n$ ) and on the incident and transmitted angles. As a simplified case, we may estimate  $\phi_{Rspec}$  following the normal incidence Fresnel expression [54]:

$$\phi_{Rspec} = \left( \frac{n - 1}{n + 1} \right)^2, \tag{3}$$

where  $n$  is the real part of the index of refraction. Considering dielectrics,  $\phi_{Rspec} \approx 0$  when  $n \approx 1$  (for transparent materials); and  $\phi_{Rspec}$  approaches unity for very large  $n$ . Published data for the complex refractive index ( $n-ik$ ) of POM are presented in Table 6, where  $k$  is the imaginary part of the index of refraction.

**Table 6. Refractive index at 10.6 mm**

Researcher	$n$	$k$	Method	Reference
Cooke	1.34	0.12	Kramers-Kronig calculation, Tadokoro data	[55,56]
Whittet, <i>et al.</i>	1.93	0.07	FTIR	[57]

The data reported by Whittet, *et al.* has much higher wavelength resolution, and probably has significantly better accuracy than the Cooke extrapolation from the results in Reference 56. Using the results of Whittet, *et al.*, we may calculate  $\phi_{Rspec}$  for a clean, ideal (optically flat) POM interface with air as  $\phi_{Rspec} \approx 0.1$  (applicable hereafter), implying transmissivity  $\phi_T \leq 90\%$  at best (for contrast, Cooke's results suggest  $\phi_R \approx 2\%$ ). Several studies [11,15,16,22,58] have indicated experimental results for transmission far below these values - this issue is addressed later in this section.

In any real ablation event,  $\phi_{\text{Rdiff}}$  will also play a role, further reducing  $\phi_{\text{T}}$ . Actually, for a typical commercial sample of POM, it may be the case that  $\phi_{\text{Rdiff}} > \phi_{\text{Rspec}}$ . The diffuse reflectivity  $\phi_{\text{Rdiff}}$  is more complex than the specular reflectivity, and depends on, *e.g.*, the surface roughness, the angle of incidence of the beam, and the presence of any contaminants on the target surface. In other words,  $\phi_{\text{Rdiff}}$  depends strongly on the processing of the target. This statement is not limited to the initial ‘manufactured state’ of the propellant - the surface roughness will change with the arrival of each laser pulse. Although it is possible to polish metal targets with successive laser pulses by reducing the scale size of surface effects, it appears that successive pulses on dielectric materials like POM increases, rather than decreases, the surface roughness. This is still an open topic, as the authors are not aware of any significant study of diffuse reflectivity for POM at  $\lambda = 10.6$  mm.

Considering both plasma and surface reflectivity, the ‘effective fluence’  $\Phi(0)$  passing through the target surface into the material may now be expressed as  $\Phi(0) = \chi\Phi_{\text{L}} = (1-\phi_{\text{A}})(1-\phi_{\text{R}})\Phi_{\text{L}}$ . It is important to note that in the laboratory, a focused beam can produce higher fluence below the material surface than at the surface, particularly for transparent materials. Using long focal distances (relative to the width of the laser spot) will minimize such effects.

As it enters the target material, the laser pulse is absorbed and a combination of photochemical degradation and heating of the target material occurs. For heating, many treatments linking fluence to temperature reference the theory published by Carlslaw and Jaeger [59] for radiation-driven 1-D thermal transport into a semi-infinite solid. This theory is used to predict that the time-dependent temperature rise  $\Delta T(t)$  at a surface is dependent on the product of the average irradiance  $\Psi$  (in W/m<sup>2</sup>, sometimes improperly called intensity) and the square root of the product of the thermal diffusivity  $D$  and irradiation time  $t$  (for the purpose of this analysis,  $t = \tau$ , the laser pulse length), where we have used here  $\Psi \approx \Phi/\tau$ :

$$\Delta T(T) \approx \frac{2\chi\Psi}{k} \left( \frac{D\tau}{\pi} \right)^{1/2} \approx \frac{2\chi\Phi_{\text{L}}}{k} \left( \frac{D}{\pi\tau} \right)^{1/2}, \quad (4)$$

where  $\kappa$  and  $D$  are the thermal conductivity and diffusivity, respectively. This approach was echoed, *e.g.*, in major works by Anisimov [40], Ready [60] and Bäuerle [52].

Application of (4) to CO<sub>2</sub> laser ablation of POM reveals an interesting dilemma. Using the representative values  $D \approx 1 \times 10^{-7}$  m<sup>2</sup>/s and  $\kappa \approx 0.25$  W/(m K), considering the case where  $\phi_{\text{A}} \approx 0$ , and taking  $\phi_{\text{R}} \approx 0.1$ , we can express the change in temperature as  $\Delta T(\tau)$  [K]  $\approx (1.3 \times 10^{-3}) \times \Phi/\tau^{1/2}$ , where  $\Phi$  is in J/m<sup>2</sup> and  $\tau$  is in s. Typical literature studies of CO<sub>2</sub> laser ablation of POM were made with  $\tau \approx 5$   $\mu$ s and  $\Phi_{\text{L}} \approx 10^4$ - $10^6$  J/m<sup>2</sup>. Using  $\Phi_{\text{L}} \approx 10^4$  J/m<sup>2</sup>, (4) predicts surface temperatures exceeding 5000 K (*i.e.*, in the plasma regime), but in the laboratory, this fluence is barely sufficient to produce combustion of a POM target. Actually, the temperature necessary for POM combustion is only  $\sim 300$ - $500$  K [37], about one order less than predicted. Furthermore, the critical plasma threshold is not reached until  $\Phi_{\text{L}} \sim 2$ - $3 \times 10^5$  J/m<sup>2</sup>, probably corresponding to temperatures of around 10,000 K at the target.

Consider for a moment that the incident fluence threshold is known for both combustion and plasma. Because ablation exhaust emits significant radiation in both of these regimes, the threshold positions can be established using either conventional or time-resolved photographic techniques. The corresponding threshold temperatures are also known, as established above. Both of these temperatures fall short of the predictions of (4), which does not account for plasma or reflectivity, apparently by a factor of  $\approx 10$ . Since (4) indicates a direct dependence of the surface temperature on the incident fluence, we may infer that the product  $(1-\phi_{\text{A}})(1-\phi_{\text{R}})$ , which reduces the incident fluence, is on the order of 10%. This value is consistent with several of the experimental reports in the literature. For instance, experimental pinhole transmission studies by Sterling [16] indicated  $\phi_{\text{T}} \approx 0.1$  when both vapor and plasma were present, but a fluence-dependent treatment was not conducted, and the fluence used in the experiment is unclear. Pinhole transmission experiments conducted at DLR indicated more optimistic values of  $\phi_{\text{T}} \approx 35$ - $55\%$  [11,58]. The DLR pulse was strongly affected by plasma attenuation, as confirmed by time-resolved measurements of  $\phi_{\text{R}}$  and  $\phi_{\text{T}}$ . A very low value of  $\phi_{\text{T}} \sim 7\%$  was reported by Sinko [22], based on modeling of experimental measurements of CO<sub>2</sub> laser ablation mass removal and impulse in the vaporization regime. The model did not account for plasma, and the data considered

during the parameter fitting was all below the plasma threshold, so plasma absorption probably does not account for the difference. The low result may stem from the model assumption that all non-reflected energy in the laser pulse was transferred into exhaust kinetic energy. Significant energy is probably also transferred into various vibrational, thermal, and rotational energy modes in the exhaust; in addition, ablation exhaust is not perfectly collimated, and these effects were not considered in the model. In striking contrast to the above results, Beckel [49] reported 92% transmission during cw irradiation of POM by a CO<sub>2</sub> laser, a value roughly of the same magnitude as the theoretical values predicted from the normal-incidence Fresnel relations. Resolving this discrepancy is very important for future analysis of laser ablation, but so far the path to do so is not clear.

As a final note on this subject,  $\phi_R$  also depends on the relative polarization of the laser beam and the polymer surface. Most commercial polymer materials exhibit some degree of polarization anisotropy, as indicated, *e.g.*, in the published results of Tadokoro, *et al.* [56]. The output of CO<sub>2</sub> lasers usually also exhibits partial polarization. Hypothetically, better or worse ablation performance (*e.g.*, mass loss and impulse generation) can be achieved using the same beam and the same sample, merely by changing the relative alignment of the target with the laser to adjust the polarization direction.

### 1.5 Absorption coefficient

As shown in the preceding section, the optical properties of the target strongly influence the energy delivery into the target. At the present state of understanding, the most important optical properties are the fluence  $\Phi$ , reflectivity  $\phi_R$ , and absorption coefficient  $\alpha$ . Fluence and reflectivity were discussed above, and  $\alpha$  can be theoretically calculated at a wavelength of  $\lambda = 10.6 \mu\text{m}$  by using the real and imaginary parts of the refractive index ( $n$  and  $k$ , respectively) [52]:

$$\alpha = \frac{4\pi nk}{\lambda} . \quad (5)$$

Using the values of Whittet, *et al.* in Table 6, we may use (5) to estimate  $\alpha \approx 1.9 \times 10^5 \text{ m}^{-1}$  (for  $\lambda = 10.6 \mu\text{m}$ ). Cooke's values, based on the data of Tadokoro, *et al.*, correspond to  $\alpha \approx 1.6 \times 10^5 \text{ m}^{-1}$ . These values are generally consistent with the more direct experimental measurements of  $a$  presented in Table 7, but surprisingly, they appear to differ from the values of  $a$  reported by the same authors at  $\lambda = 10.6 \text{ mm}$ .

**Table 7. Absorption coefficient  $\alpha$  at  $\lambda = 10.6 \mu\text{m}$**

Researcher	$\alpha [\text{m}^{-1}] (10.6\mu\text{m})$	Method	Reference
Tadokoro, <i>et al.</i>	$6.6 \times 10^5$	FTIR, $E_{\perp}$ (absolute)	[56]
	$9.3 \times 10^5$	FTIR, $E_{\parallel}$ (absolute)	
	$2.63 \times 10^5$	FTIR, $E_{\perp}$ (absolute)	
	$5.3 \times 10^5$	FTIR, $E_{\parallel}$ (absolute)	
Whittet, <i>et al.</i>	$1.308 \times 10^5$	FTIR (absolute)	[57]
	$9.84 \times 10^4$	FTIR (absolute)	
Cooke	$3.4 \times 10^5$	FTIR (absolute)	[55]
Beckel	$7.5 \times 10^3$	FTIR (absolute)	[49]
Reilly	$\sim 4 \times 10^5$	FTIR (absolute)	[7]
	$\sim 1 \times 10^5$	Ablated depth (effective)	
Sinko, <i>et al.</i>	$6.74 \pm 0.24 \times 10^5$	Micro-FTIR (absolute)	[15]
Sinko	$1.92 \pm 0.23 \times 10^5$	Ablation model fitting (effective)	[22]

Some additional discussion is merited regarding the absorption coefficient. One of the principal reasons for the good ablation performance of POM is the serendipitous alignment of its infrared absorption bands with the  $\lambda = 10.6 \mu\text{m}$  ( $9.43 \times 10^4 \text{ m}^{-1}$ ) spectral peak from the (001) $\rightarrow$ (100) vibrational transition most commonly used for CO<sub>2</sub> lasers [61]. The molecular vibrations of POM responsible for

these bands are the C-O-C symmetric stretch and C-H<sub>2</sub> rocking vibration, which make up respectively about 75% and 25% of the absorption peak in the FTIR spectrum [56]. Absorption in POM is shown in Figure 6, as measured by microscopic Fourier Transform Infrared (FTIR) Spectroscopy on a Delrin® homopolymer. The data in Figure 6 was previously reported [15,22] in terms of percent transmission, but new insight may be gained by discussing those results directly in terms of the absorption coefficient  $\alpha$ .

It is important to point out that thermal effects may alter  $\alpha$  significantly during the laser pulse arrival, and in general, such effects depend on the laser pulse length. Reported values for  $a$  are summarized in Table 7.

So far, no study directly compared the FTIR of homopolymer and copolymer POM varieties, and it is unclear at this stage whether stabilization of the POM chain significantly affects the absorption coefficient. One may anticipate that the absorption will differ somewhat based on the specific chemical structure of the chosen copolymer.

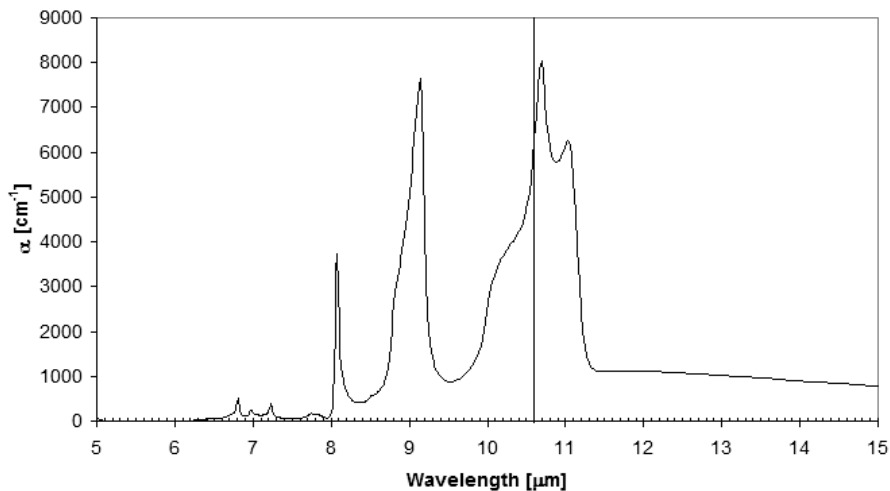


Figure 6. FTIR spectrum of  $\alpha(\lambda)$  compared to  $\lambda = 10.6$  CO<sub>2</sub> laser wavelength. Microscopic FTIR of  $\approx 4$  mm thick homopolymer POM sample at room temperature was provided by Jane Zhu, Kenneth Potts, Stewart Millen, and Robert Sinko of Eastman Chemical Company (Kingsport, TN).

Another good CO<sub>2</sub> laser wavelength range for POM ablation can be expected around  $\lambda \approx 9$  mm ( $\approx 1.1 \times 10^5$  m<sup>-1</sup>). Tadokoro, *et al.* [56] reported bands at  $1.091 \times 10^5$  m<sup>-1</sup> (9.2  $\mu$ m) from C-O-C asymmetric stretching (70%) and O-C-O bending (26%) modes; and, at  $1.097 \times 10^5$  m<sup>-1</sup> (9.1  $\mu$ m) from C-O-C asymmetric stretching (77%) and CH<sub>2</sub> rocking modes (19%). A laser line centered at  $\approx 8.9$ -9.3 mm would at least intersect a shoulder of one of these peaks. It should be noted that CO<sub>2</sub> lasers operating at  $\lambda \approx 9$  mm are already in common use for industrial cutting applications [62], so an interesting study would be to compare laser ablation at the same energy between the two wavelengths. If the CO<sub>2</sub> laser radiation is directly coupling to the vibrational bands in POM, a study of this type would demonstrate the possibility of discriminating between symmetric and asymmetric stretches during ablation merely by altering the irradiation wavelength. It is possible that this selective effect could have a dramatic effect on ablation processes, particularly at low fluence.

For laser propulsion, many studies sought to use  $a$  as a control parameter to influence the specific impulse ( $I_{sp}$ ) in order to more efficiently consume propellant. However, large absorption does not always correspond to high  $I_{sp}$  (and low ablated mass). Strong absorption can also lead to deep ablation of material following significant energy deposition, and *increased* mass removal. Doping can also have an effect on  $\alpha$ , for instance, the increased absorption associated with carbon-doped ( $\sim 1$ -3%) POM samples was reported at about 5% [22]. Beckel's reported value for  $\alpha$  seems anomalously low compared to values reported by other researchers. The differences between irradiation times used in the various experiments may help to explain the discrepancies between the reported values, but a more careful study of the reflection and transmission from polyoxymethylene is necessary to close the topic.

Now that both thermal and optical (*i.e.*, photochemical) pathways have been described in some detail, it will be instructive to compare these mechanisms. Several analytical approaches have been put forward recently to address ablation modeling for impulse generation in polymers [22,40, 52,60,63-65]

and specifically for modeling CO<sub>2</sub> laser ablation of POM [22,63,64]. Such models typically either address imparted impulse directly, or approach impulse production through pressure formation.

### 5.1 Mass Removal and Impulse Models

Two major regimes are recognized for laser ablation impulse generation, the vaporization and plasma regimes. In the vaporization regime, the fluence is sufficient to vaporize the target material, but plasma shielding is unimportant; *i.e.*,  $\phi_A \approx 0$ . It remains unclear whether the best modeling approach to impulse generation in the vaporization regime is via rocket-like thrust or via the vaporization pressure above the target. The plasma regime includes fluences where both vaporization and plasma occur, where  $\phi_A$  is non-negligible. In the plasma regime, the majority of imparted impulse is from the plasma pressure.

In the vaporization regime, treatment of imparted impulse by conservation of momentum seems appropriate, as long as the interaction occurs under vacuum, where effects from the ambient atmosphere are minimized (for instance, redeposition of ablated material back onto the surface). However, we note that in some cases, atmospheric confinement may increase the interaction time between exhaust and target, increasing total delivered impulse. These effects are not yet fully understood or adequately accounted for in impulse modeling efforts using atmospheric conditions. An experimental effort by Anju [17] to examine time-dependent and pressure-based effects on ablation, using an interferometric system, concluded that the only differences between air and vacuum conditions were due to plasma shielding. The remainder of this section will concern impulse modeling in vacuum; however, at least some literature evidence [22] suggests that such models can be successfully applied to atmospheric ablation, as well.

### 5.2 Photochemical Mass Removal

Photochemical ablation has been described in detail by Bäuerle [52], and is governed by the Bouguer-Lambert-Beer absorption law [66]:

$$\Phi(z) = \Phi(0) e^{-\alpha z}, \tag{6}$$

where we note that  $\Phi(0) = \Phi_L(1-\phi_A)(1-\phi_R) = \chi \Phi_L$ . By inverting (6), we may express the optical threshold ablation depth  $z_a$  in terms of the threshold fluence for ablation  $\Phi_a$ , as  $z_a = z(\Phi_a)$ . By a threshold fluence for ablation, we mean the fluence at which significant ablation is observed, also known as the ablation threshold. In practice, exceeding  $\Phi_a$  results in, *e.g.*, a sharp rise in vaporized material and ablated mass. We may approximate a characteristic absorption depth as  $z_a \approx 1/\alpha$ , so for the typical values in Table 7 ( $\alpha \approx 10^5$ - $10^6$  m<sup>-1</sup>), we expect a threshold depth on the order of 1-10 mm. The total ablated mass  $m$  is the product of the target density, the spot area, and the threshold depth. The ablated mass per spot area ( $\mu$ ), also called the ablated mass areal density, is:

$$\mu(\Phi) = \frac{m(\Phi)}{a} = \frac{\rho}{\alpha} \ln \frac{\Phi(0)}{\Phi_a}. \tag{7}$$

As  $\Phi \rightarrow \infty$ , we may expect that  $\mu \rightarrow \infty$ , unless the effect of plasma shielding is taken into account.

Photochemical modeling is typically applied to materials irradiated with at most ns-scale UV or visible laser pulses; however, it appears to be a valid approximation for CO<sub>2</sub> laser ablation when the pulse length is sufficiently short and  $\alpha$  is not too large. It may be mentioned here that the bond energy of the C-O bond linking -CH<sub>2</sub>O- monomer units has been given as  $\approx 6 \times 10^{-19}$  J [67]. Each CO<sub>2</sub> laser photon carries  $\approx 1.88 \times 10^{-20}$  J. Since the reaction proceeds from the chain ends, only one bond need be broken to liberate monomer (*i.e.*, formaldehyde). Each broken bond would require a minimum of about 32 CO<sub>2</sub> laser photons to support a photochemical process.

### 5.3 Photothermal Mass Removal

The photothermal ablation process has been outlined by Bäuerle based on an expression in Reference 52 for temperature distribution under irradiation. The 1-dimensional version of this expression, applied to longitudinal heat diffusion with a temporal rectangular pulse, is:

$$T(t, z) \approx \frac{\Phi(0)}{\rho c_p \sqrt{4\pi D t}} e^{-\frac{z^2}{4Dt}}. \quad (8)$$

Using  $t = \tau$  to determine the state at the end of the laser pulse, assuming the total energy release is equivalent to the part of the laser pulse energy that passes into the surface, and inverting (8) to find the depth  $z$  at which the boiling temperature  $T_b$  is reached, we have:

$$z(T) \approx \sqrt{4D\tau \ln \left( \frac{\Phi(0)}{\rho c_p \sqrt{4\pi D \tau T_b}} \right)}. \quad (9)$$

We may now express ablated mass areal density as the product of density and ablated depth:

$$\mu \approx 2\rho \sqrt{D\tau \ln \left( \frac{(1-\phi_R)(1-\phi_A)\Phi_L}{2\rho c_p \sqrt{\pi D \tau T_b}} \right)} = 2\rho \sqrt{D\tau \ln \left( \frac{\Phi_L}{\Phi_a} \right)}. \quad (10)$$

Despite the plethora of constants, as shown on the right, the expression in (10) has a relatively straightforward dependence on  $\Phi$ . Equation 10 implies a thermal threshold fluence:

$$\Phi_a = \frac{2\rho c_p T_b \sqrt{\pi D \tau}}{(1-\phi_R)(1-\phi_A)}. \quad (11)$$

We may calculate this threshold fluence using the representative thermal data chosen earlier. Assuming  $\rho \approx 1.42 \times 10^3 \text{ kg/m}^3$ ,  $c_p \approx 1500 \text{ J/(kg K)}$ ,  $D \approx 4 \times 10^{-8} \text{ m}^2/\text{s}$ ,  $\tau \approx 10 \text{ } \mu\text{s}$ ,  $T_b \approx 500 \text{ K}$ ,  $\phi_R \approx 0.1$ , and  $\phi_A = 0$ , we find  $\Phi_a \approx 2.6 \times 10^3 \text{ J/m}^2$ . This compares favorably with the experimental value  $\Phi_a \approx 2 \times 10^3 \text{ J/m}^2$  previously reported by Reilly [7]. We therefore choose the representative value  $F_a \approx 0.25 \text{ J/cm}^2$  for application to models discussed in this paper. As with the photochemical case,  $\mu \rightarrow \infty$  when  $\Phi_a \rightarrow 0$  and when  $\Phi_L \rightarrow \infty$ .

#### 5.4 Comparing Photochemical and Photothermal Pathways

An intermediate treatment of ablation was discussed by Bäuerle as a way to synthesize photochemical and photothermal ablation pathways for more accurate modeling [52]. A separate, but similar, approach by Srinivisan, *et al.* [68] used the addition of photochemical and photothermal terms to form a total ablated depth. This logic may also be applied to the expressions in Sections 1.5 and 1.6.

To gauge the importance of photochemical and photothermal effects for a certain combination of a material and laser system, characteristic values of  $z_a$  corresponding to  $\Phi_a$  are often compared. For photochemical ablation, the expression is  $z_a \approx 1/\alpha$ , and for photothermal ablation, a characteristic thermal diffusion parameter is often used:  $z_a \approx (4 D \tau)^{1/2}$  [52]. These parameters suggest three regimes of operation, which correspond to the photochemical, intermediate (or in Bäuerle's terminology, 'photophysical' [52]), and photothermal regimes as mentioned before:

$$2\alpha\sqrt{D\tau} \begin{cases} < 1 & \text{Photochemical} \\ \sim 1 & \text{Intermediate} \\ > 1 & \text{Photothermal} \end{cases} \quad (12)$$

Unfortunately, there is no obvious connection based on  $2\alpha(D\tau)^{1/2}$  which links the models in (10) to the plasma regime. Later, we will discuss a method of connecting the plasma and vaporization regimes, proposed in Reference 65.

For photochemical ablation of POM, reasonable limits on  $\alpha$  for  $\text{CO}_2$  radiation in POM apparently range from about  $10^5$ - $10^6 \text{ m}^{-1}$ , indicating a characteristic photochemical ablation depth  $z_a \sim 1$ - $10 \text{ mm}$ . For lasers with pulse lengths  $< 5 \text{ mm}$  and targets with moderate absorption  $\alpha \sim 2 \times 10^5 \text{ m}^{-1}$ , the photochemical component would be expected to dominate; in the latter conditions, for practical application, thermal diffusion effects are insignificant.

However, many photons are required in order to break a single polymer bond ( $\approx 30$  per C-O bond). Assuming this is still possible, high fluence would seem to be needed. Thus, it is conceivable that thermally-driven ablation might be supported at low fluence, and we must make a careful consideration of the laser pulse length. Typical  $\text{CO}_2$  laser pulses have a short, high-fluence initial pulse of about 50-150 ns full width at half maximum (FWHM) which is generally followed immediately by a longer tail that lasts about 5-15  $\mu\text{s}$  (e.g., time until 90% of total energy), usually (but not always) at lower fluence than the main pulse. An example of a typical laser pulse is shown in Figure 7.

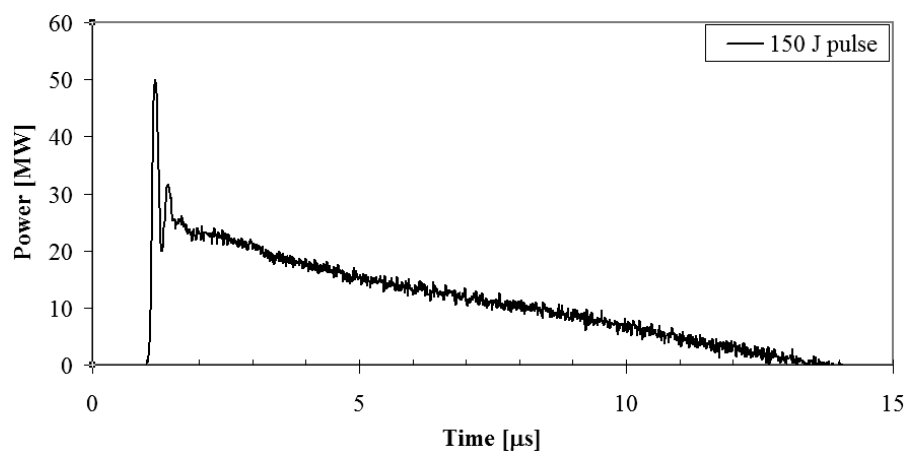


Figure 7. A typical  $\text{CO}_2$  laser pulse (courtesy Stefan Scharring, DLR-Stuttgart, Germany)

The percentage of the laser pulse energy carried by the peak vs. the tail becomes important in a consideration of the pulse length, especially when considering plasma shielding. For the systems in this study, generally only 10-30% of the total pulse energy is in the  $\sim 100 \text{ ns}$  main pulse.

For photothermal ablation,  $z_a \sim 1 \mu\text{m}$  for  $\tau \approx 6$ - $7 \text{ ms}$ . In general, this is less than the photochemical depth mentioned above; however, thermal effects will still be important for  $\text{CO}_2$  laser ablation of POM using moderate to long laser pulse lengths (i.e., about  $\tau \sim 5 \text{ ms}$  or greater). The photothermal threshold depth varies only slowly, as  $\tau^{1/2}$ , so even for the longest pulse lengths of about 15 ms,  $z_a \sim 2 \text{ mm}$ . Therefore, photothermal effects have, at most, approximately equal importance with optical effects in this ablation regime. Representative values for some existing experimental laser devices are presented below in the next section.

### 3. EXPERIMENTAL ENVIRONMENT

The ablation of POM is dependent not only on the material and its properties, but also on the particular experimental conditions used in a given study. The most important considerations are the  $\text{CO}_2$  laser used, the test environment, and material conditioning effects.

#### 3.1 $\text{CO}_2$ Lasers

This section provides a basic comparison of the laser systems that produced the data assembled in this study. More details can be found in the original works. Institutions include the former AVCO Everett (AVCO) research lab at Everett, MA, USA; the Air Force Research Laboratory (AFRL) at Edwards Air Force Base, CA, USA; The German Aerospace Center (Deutsches Zentrum für Luft und Raumfahrt, DLR) at Stuttgart, Germany; Nagoya University (NU), Nagoya, Japan; Sosnovy-Bor (SBOR) in the Leningrad region, Russia; Tohoku University (TU), Sendai, Japan; and the University of Alabama in

Huntsville (UAH), Huntsville, AL, USA. Studies include single-shot (AVCO [7,8], DLR [9-12,58], NU [17-20], TU [13,14], UAH [15,16,22,23]), bursts of rp pulses (AFRL [4,70], AVCO [7], DLR [71,72], NU [18,19], and SBOR [21,24]) and even cw operation (SBOR [21,24]). The NU laser was manufactured by Selective Laser Coating Removal - LaserTechnik, GmbH (Germany) and the TU laser by the General Physics Institute (Moscow, Russia). The laser system parameters are outlined in Table 8.

**Table 8. Key Parameters of the Laser Systems Considered in this Study**

Group	Laser	$E_L$ [J]	$f$ Hz	$\theta_d$ [mrad]	$\tau^{**}$ [ns]	$\tau^{***}$ [ $\mu$ s]	Source
AFRL	AVCO HPPL-300	50-400	25	$\sim 0.06$	10-30	18-25	[4,70]
AVCO	Lumonics 601	$\approx 20$	*	$\sim 10$	$\approx 15$	$\approx 1$	[7]
	Lumonics 602	$\sim 85$	*	$\sim 7$	$\approx 50$	$\approx 1$	[7]
	Scale-Up	$\sim 1000$	*	*	600	$\approx 3-5$	[7]
DLR	Multispectral laser	$\leq 310$	$\leq 50$	$\approx 4$	$\sim 200$	5-30	[9,71]
		$\leq 410$	$\leq 45$	0.5	$\sim 200$	5-30	[9]
NU	SLCR ML 205E	$\leq 10.3$	$\leq 50$	*	140-170	3-10	[17-20]
SBOR	e-ion CO <sub>2</sub> laser	$\leq 180$	$< 50$	*	$\sim 500$	5-15	[21,24,73]
TU	GPI TC-300	23-390	*	*	50	2.5	[13,14]
UAH	Lumonics TEA-103A	$\leq 20$	$\leq 0.5$	$\approx 3$	$\approx 70$	3-5	[15,74]

\*To the authors' knowledge, the value has not been published and is not known

\*\*Main pulse, full width at half-maximum

\*\*\*Tail, time at which 90% of total energy was delivered

†Unstable resonator configuration

AFRL and SBOR both used lasers in rp mode at average powers of up to  $\approx 10$  kW. The SBOR laser could operate at about 20 kW cw. The 100 J-class and kJ-class CO<sub>2</sub> lasers were generally operated as unstable oscillators; however, the DLR laser could be operated in either a stable or unstable oscillator configuration [9]. Studies at DLR and SBOR generally used a radial ablation geometry (using Bohn bell and laser jet engine-type vehicles, respectively), and some studies of the Myrabo-type lightcraft were conducted using ablation of a toroidal ring of POM [9]. All other studies, even those incorporating nozzles, were performed on flat targets. One major difference is in the pulse profiles of the various lasers, as illustrated in Figure 8.

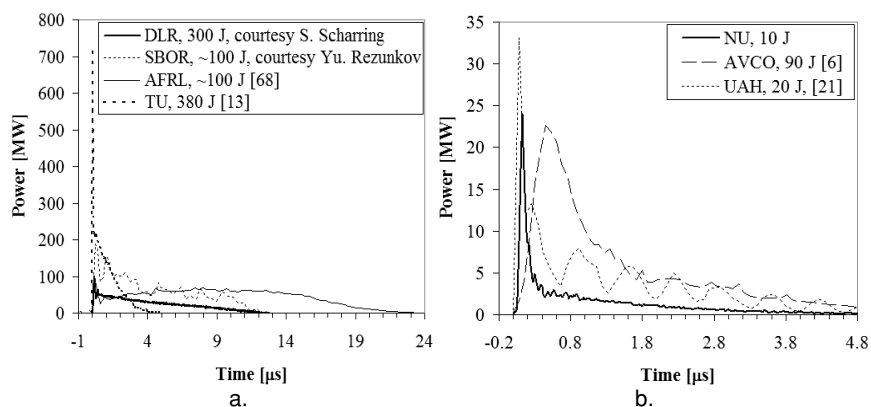


Figure 8. Pulse profiles of the various lasers in this study, [a]  $\sim 100$ -1000 J-class, and [b]  $\sim 10$ -100 J-class. The UAH laser output appears to have strong oscillations; however, this is probably due to the detection method, rather than representing the actual beam profile.

The differences arise from the excitation mechanisms used, as well as the specific gas mixtures. The DLR laser, the Scale Up system used by AVCO, and the AFRL and SBOR lasers used electron ionization excitation of the gain medium. The NU TEA CO<sub>2</sub> laser incorporates 2 capacitors along an excitation tube perpendicular to the main laser cavity. The UAH TEA CO<sub>2</sub> laser is an in-line system with 3 capacitors. Obviously, a wide variety of lasers are represented by the various groups.

In Figure 8a, it is evident that the AFRL laser has the longest pulse, mostly made up of the <sup>a</sup>20-25 ms-long tail. The DLR and SBOR lasers are quite similar to each other in pulse length and magnitude. The TU laser is particularly interesting due to its very short pulse length coupled with high peak power. In Figure 8b, lower energy laser systems are compared.

### 3.2 Ambient Condition

The ambient conditions can affect laser ablation in several ways. Some thermodynamic parameters change at increased pressure (for instance, specific heat [51], which is an important parameter in the Phipps model for vaporization-driven ablation [64]). When the ambient pressure is high, the mechanical impedance of the ambient gas can also affect the impulse, a kind of confinement effect. The threshold fluence for plasma formation also depends on the ambient pressure [52]. As discussed in more detail later, the ambient pressure of the ablation event, even in vacuum conditions, can affect the impulse generation and mass removal.

Redeposition is the net effect of deposition and condensation onto the ablated target of previously ejected particles and exhaust. This process is driven via confinement by the ambient gas, which impedes transport away from the surface, and the effect is increased when the ambient pressure is high [52]. At low fluence, large clusters can be redeposited on the surface, which can significantly affect the impulse generation and mass removal. At low pressures, redeposition is expected to be negligible [18]. It may be necessary to turn to tribological analysis to determine whether significant redeposition is occurring in a given application.

Contaminants in the chosen atmosphere can also affect ablation. For CO<sub>2</sub> laser radiation, water vapor in the air can significantly attenuate a beam over long distances. However, for the experimental scale lengths published in the literature (typically several meters), and reasonable limits of humidity in a laboratory environment, this issue is unimportant. Other contaminants can play an important role. For instance, dust and similar particles can act as ignition sites for plasma, either on the surface or above the target, unpredictably promoting plasma shielding. Such particles and exhausted gases can also contribute to beam attenuation before the arrival of the pulse at the target. For these reasons, a clean laboratory environment can minimize, but not eliminate, such effects.

There are various applications for POM in a space environment, where effects from ionizing radiation [75-77] and exposure to atomic oxygen [78] are important. References 76 and 77 examine photochemical degradation pathways driven by UV radiation. Degradation of POM by atomic oxygen [78] is another pathway which will probably need to be addressed before POM propellant could be used around LEO altitudes for long periods of time. High vacuum induces outgassing and evaporation. The various degradation pathways can be inhibited, for instance, by protecting the propellant surface, providing adequate heat dissipation, and using additives to enhance the resistance to degradation from ionizing radiation.

Impulse performance strongly depends on the ambient pressure. If a sufficient amount of residual gas is generated in the test chamber, subsequent ablation will be affected in particular in a small test chamber and modest vacuum pumping capability [18]. The choices of vacuum chamber and vacuum pumps for an experiment are therefore important considerations. Some differences will be evident between ablation in chambers of different sizes, even for the same target material and laser. Regardless of whether the experiment is in air or vacuum, if the chamber size is too small, the ablation process will cause an increase in the ambient pressure with each shot. In addition, use of too small of a chamber may distort data based on reflection of shock waves, interaction of the plume with the wall, *etc.* If the experiments are conducted under vacuum, the parity of the vacuum pump (on or off) as well as the pumping speed should also make a significant difference from the standpoint of characteristic timescales for pressure buildup and removal.

### 3.3 Conditioning Effects

The surface condition of the POM ablation target should be expected to strongly influence ablation by way of the reflectivity. POM target surfaces are often prepared by machining, which can leave metal

fragments, oils, grooves, *etc.* that respond differently to incoming laser radiation than a flat (*i.e.*, ‘optically flat’) surface of the pure polymer. This deviation in behavior will be particularly noticeable in the first few pulses. For metals, melting and surface conditioning are known to eventually reduce irregularities and surface roughness [69] with each subsequent shot, in turn reducing the diffuse components of reflection. For dielectric materials such as POM, the trend seems to be reversed; each successive laser shot probably increases the surface roughness [79]. Studies are now underway to quantify the surface changes. The absorption of the surface is also expected to increase with successive shots [52]. It is possible that there is almost no net effect resulting from this kind of simultaneous modification of reflectivity and absorption.

In addition to geometric surface considerations, groups in Japan [18,20] and Germany (pp. 24-25 of Reference 11) previously reported the necessity of making about 2-10 initial shots at the target before commencing experiments. After these first shots, the impulse was much more stable on a shot-to-shot basis. The ‘cleaning shots’ probably remove material left over from production and processing (*e.g.*, solvents, catalysts, metal fragments, and machine oils), exuded material trapped in the polymer matrix (*e.g.*, water, short-chain polymer fragments, and CH<sub>2</sub>O monomer), and post-processing environmental contaminants (*e.g.*, dust, grease, and water). The thermal analysis of POM by Duan [46] indicated that initial heating often released water. Since water has a lower vaporization temperature than POM, the initial shots likely preferentially ablate water in the POM target. After the water is removed, ablation of free monomer and POM chain fragments will be accomplished with subsequent shots.

Suzuki, *et al.* [18] showed that the conditioning effect includes a quick stabilization effect within 1-10 shots, giving way to long-term growth in the coupling as the number of shots increases. The latter effect is likely a result of crater formation in the target surface. The change in geometry can concentrate exhaust and increase the interaction area of the laser beam (thereby slightly reducing the effective fluence of the laser beam), leading to longer interaction time with the target and greater impulse. Sinko previously demonstrated a similar effect on water related to the surface concavity [80]. Although such geometric effects are important, a straightforward analysis of impulse generation remains a challenging subject.

From the above discussion, it is clear that conditioning effects cannot be neglected. This must be considered when examining literature data; for instance, apart from eliminating outliers, no effort was made to account for conditioning trends during the POM ablation studies at UAH [15,22], which often used an average of the first 5-10 shots for measurements. Conversely, both DLR and NU made several (~1-3 and ~5-10, respectively) preliminary or “cleaning shots” before recording experimental ablation data. Therefore, the values obtained at UAH may be expected to be slightly low compared to NU and DLR values, and more closely represent initial ablation effects. Experiments by Ageichik, *et al.* [21] employing cw- and rp-mode ablation are probably almost immune from these effects due to long irradiation times and large pulse numbers, respectively. The work reported by Myrabo, *et al.*, [4] was performed in rp mode, so conditioning effects would be limited to the first few shots; nevertheless, for small bursts of shots, with the number of pulses  $N < 10$ , conditioning effects may still have been significant.

#### 4. MEASUREMENT TECHNIQUES

One motivation for this study is that by testing ablation of POM with a wide range of beam shapes and quality factors, using the same equipment, some test of the dependence of the ablation results may be made on laser source parameters such as spatial and temporal distributions and durations, output spectra, and cavity stability. In order to accomplish this aim, accurate measurement is crucial. The measurement systems used by laser propulsion groups to record the major experimental parameters, namely imparted impulse and ablated mass, use many different mechanisms, which will be briefly discussed below.

##### 4.1 Ablated Mass

Ablated mass is usually measured by recording a sample material before and after an ablation shot. However, sample conditioning effects must be considered when making these measurements, as discussed earlier. It is possible to measure the ablated mass in vacuum conditions, but this is rather difficult without breaking vacuum (because, for example, the isolation imposed by the vacuum chamber and static buildup on components). As a result, experimental apparatus for vacuum pressure measurement is prohibitively expensive, and anyway, would likely be impaired by long-term accumulation of condensed exhaust from laser propulsion experiments.

A second method is to record the change in pressure in a vacuum chamber following ablation. Unfortunately, the size of the vacuum chamber can introduce significant uncertainty to this type of measurement, and is also problematic since many of the ablatants may be expected to condense out onto the lower-temperature chamber walls, rather than remaining in the vapor phase long enough for a measurement to be valid. Finally, the temperature of the ablated gas is not expected to be the same as the ambient environment. Therefore this method is not recommended.

Finally, as a third option, surface profilometry can be used to geometrically construct the volume of the ablation crater. So far, to the authors' knowledge, this technique was not used for studies of CO<sub>2</sub> laser ablation of POM. Surface profiling is generally time-consuming, and requires expensive equipment; on the other hand, it appears to be a more sensitive technique for measurement of mass removal than most scientific balances. Surface profiling does not account for partial volume losses; for instance, if the effective volume of the target remains the same, but the density decreases. The latter behavior is not expected to be significant for ablation of POM.

Clearly, there exists a need for some inexpensive measurement technique for fine measurement of mass to be used for laser ablation propulsion research applications, particularly in vacuum. At the present time, the best equipment for this purpose is probably still the laboratory balance, but if fine resolution is needed, surface profiling is a good option.

## 4.2 Imparted Impulse

Unlike the situation for measurement of ablated mass, there are many techniques in widespread use for measurement of imparted impulse.

The most common technique involves the use of an impulse pendulum. Sometimes such devices are referred to as ballistic pendulums, but in fact this is not strictly correct, as historically, a ballistic pendulum stops a moving target, converting its momentum into potential energy. In modern impulse pendulums, the target is initially stationary, and affixed to the pendulum. However, an impulse pendulum can be used as a ballistic pendulum in the limit where momentum from absorption of photons dominates. Several impulse pendulum systems have been used to study CO<sub>2</sub> laser ablation of POM, including systems constructed by AFRL [81,82], DLR [9] and UAH [16].

The next most common technique for measurement of impulse has been the launch and subsequent observation of targets. Various configurations have been tried including horizontal [13] and vertical [4,9-12,58] launches with POM targets. Horizontal, wire-guided tests have also been performed [24]. Care must be taken in launch experiments to avoid significant pressure build-up between the launchpad and the target. One method of avoiding such effects is the use of a prong-like launchpad structure to allow quick diffusion of any built-up pressure [71]. Such pressure can enhance the imparted impulse, but does not represent accurate flight conditions. Watanabe, *et al.* [13] used an aperture of roughly the same size as the target during horizontal launches, and it is possible that some interaction occurred between the launchpad and target due to pressure buildup. After launch, literature trajectory measurements included optical rangefinding [71], optical interruption [13], and imaging [4] strategies.

Torsion balances are commonly used for impulse measurement. Although the accuracy is very good, significant time must be invested in proper calibration, and also for normal use during measurements, as the motion of the system must damp out before another measurement can be made. The choice of the rotational support (*e.g.*, pivot, bearings, knife edge) is therefore very important. Especially for large load masses, the effect of friction on the pivot mechanism can be significant, as can the effects from unintended degrees of freedom present in the motion of the arms of the torsion pendulum. At least two groups used torsion balances for impulse measurement with a POM propellant [18,83].

Piezoelectric force sensors were used for impulse measurement from CO<sub>2</sub> laser ablation of POM, primarily by UAH [15,16,22,23]. Some details of this technique were treated by Sinko and Lassiter [84]. A force sensor can accurately report time-resolved compression of a target material against the sensor if the compression time is sufficiently longer than the response time of the sensor, allowing recovery of the imparted impulse. Force sensors are best used with polymer targets to avoid strong oscillations arising from acoustic impedance matching. Force sensor output is acceptable for use in measuring total imparted impulse, and usually a given sensor will cover 3-4 orders of magnitude of impulse generation if careful treatment is made. Current technology enables measurement down to 100's of nNs, limited by the sensor's signal to noise ratio in a given experimental environment. Hardened impact sensors can withstand kN-level forces and accurately measure impulse in excess of Ns. Typical rise times on the order of 10 ms are common. Practical use of the sensors often requires

Fast Fourier Transform post-processing and subsequent integration of the force signal to generate impulse data. However, even with these additional steps, use of force sensors usually enables rapid measurement, since multiple shots can be taken with very little delay (typical charge-leakage time constants are on the order of 10-100 s). Piezoelectric sensors can also be used under vacuum conditions as long as the maximum tensile load of the sensor is not exceeded.

The Velocity Interferometer System for Any Reflector (VISAR) has been successfully applied to measure time-resolved force at NU [20] for thin film ablation targets backed by a reflective surface, including study of POM targets. Unfortunately, the VISAR technique measured only a local impulse, and was not spatially-integrated. Therefore, although the results are useful for determination of the time-dependence of force generation, they are not representative of the total impulse. Thus, direct comparison between VISAR data and other results needs additional diagnostics, including numerical simulation. It is ironic that most force sensors fail to resolve the time-resolved ablative forces, while VISAR cannot measure the total impulse. The two techniques are somewhat complementary, and used in conjunction, can thoroughly specify the spatial- and time-resolved ablative behavior. It is possible that further development of these techniques may yield additional information - for instance, inference of an ablative force from force sensor data, or the use of a line VISAR technique.

Regardless of which techniques are used, researchers should probably use at least two independent measurement techniques in order to provide proper validation of their experimental results for imparted impulse. Measurement limits for imparted impulse are set by the techniques, and differences or biases between techniques should be accounted for in any accurate report of laser ablation impulse. This is even true between two studies using the same technique. For instance, the AFRL-DLR study on lightcraft [9] used two different impulse pendula, and reported significant measurement discrepancies between the results during calibration. Sinko [80] recently found discrepancies in impulse measurements of CO<sub>2</sub> laser ablation of bulk water samples made between different force sensors. The study in Reference 84 directly compared results from an impulse pendulum and force sensors, in that case finding good agreement between measurements of ablation of polychlorotrifluoroethylene.

### 4.3 Laser Pulse Energy

Energy measurement of CO<sub>2</sub> laser output is made more difficult by the long wavelength. Common solutions for high fluence beams up to about 10<sup>5</sup> J/m<sup>2</sup> include thermopile detectors and pyrometers. Other solutions include photon drag detectors (for low fluence) and some types of photodiodes. Often it was seen to be necessary to reduce the fluence of the laser beam before it reached the detectors by some known factor, for instance attenuating the beam by transmission, or by measuring reflections from optics. The initial studies on CO<sub>2</sub> laser ablation of POM conducted by AVCO used pyrometers with a damage threshold below 10<sup>4</sup> J/m<sup>2</sup> to measure a beam fluence above this limit by transmitting the pulse through a 4mm-thick CaF window [7]. AVCO also used two thermopile-type calorimeters, one with a black paint coating with a damage threshold around 5×10<sup>3</sup> J/m<sup>2</sup> and the other, with a reflective PTFE coating, with a threshold of about 2×10<sup>4</sup> J/m<sup>2</sup>. This range of thresholds is still typical of most CO<sub>2</sub> laser energy detectors. Most groups (AFRL [85], AVCO, DLR, NU, and UAH) used thermopile-type detectors. SBOR used two wire bolometers to measure energy [24], and TU also used a wire bolometer [14]; operation of this type of device is further described in Reference 86.

### 4.4 Laser Spot Area

Literature spot area measurements were often performed by measuring a darkened area on heat-sensitive papers after ablation [*e.g.*, 4,9,13,18,22], however, to the authors' knowledge, no group has yet made any physical study of such paper to determine, *e.g.*, coloring and damage thresholds of the paper, or the correspondence of such information to effects on an ablation target. Nor has any group so far reported the type of paper used in such measurements. There are many types of thermally sensitive paper, and one cannot expect that all of them exhibit the same behavior under irradiation. Even assuming that their use is valid, measurement by imaging a 2-dimensional spot provides only a kind of outer contour of the laser beam. Detailed spatial structure of the beam profile is usually lost; in addition, most of these papers exhibit several levels of ablation behavior, from coloration to damage to complete destruction. The response of the paper to radiation (*e.g.*, from plasma) must also be considered in the context of the polymer. Finally, significant thermal broadening of the spot is possible long after the laser pulse. Some thermal 'papers' include plastic films that distort heavily under heating (*e.g.*, see Reference 13), complicating even these simple efforts to measure the beam spot.

Spot areas produced on polymers such as POM and PVC have also been measured [*e.g.*, see 7,15,18,22], these are probably associated with a higher fluence contour, but without additional information, suffer from the same basic limitations as those of thermal papers.

Cross-sectional characterization of the laser beam is an important step in the right direction, but can usually only be performed with an unfocused beam to avoid damaging a detector. An obvious ‘solution’, measurement after the focus, is usually unfeasible due to air breakdown near the focus, which absorbs part of the laser pulse. Although measurements could be conducted in vacuum, most energy measurement instrumentation is not designed to operate under vacuum conditions.

In the context of cross-sectional characterization, preferably full 2-D spatial profiling of the fluence of the laser beam, the contour data generated during ablation may be acceptable, if it is sufficiently accurate to simply scale the pulse shape to the profile. The pulse shape is modified when it interacts with optics. Modeling the pulse shape will then be necessary.

## 5. IMPULSE PERFORMANCE

Towards a model of impulse, we will consider the two accepted pathways (photochemical and photothermal) towards ablation. In order to form impulse, since mass removal has already been expressed, we merely need to specify the exhaust velocity. The product of the exhaust mass and the exhaust velocity forms an impulse of ablated material, and we may assume, by momentum conservation, that a momentum equal in magnitude but opposite in direction is imparted to the target. As mentioned before, there are various control parameters inherent to a given laboratory setup, which have a strong influence on ablation. We will begin the discussion with a relatively well-understood parameter, the fluence of the laser beam.

### 5.1 Fluence-Dependent Impulse Modeling in Vacuum

The approach presented here towards fluence-dependent, vaporization-driven ablation modeling is based on two physical quantities: the ablated mass and the exhaust velocity. Unfortunately, it is not the case that every particle leaving the target surface has a uniform velocity. The kinetic energy of the exhaust  $E_k$  has some distribution of velocities for a given ablation event, which suggests a method to recover a net exhaust velocity  $v_{ex}$  based on the first moment of the square of the velocity distribution (*i.e.*, energy equivalent) along the longitudinal axis,  $\langle v_z^2 \rangle$ .  $E_k$  can then be expressed in terms of  $\langle v_z^2 \rangle$ , the ablated mass  $m$ , and the incident laser pulse energy  $E_L$ , based on energy conservation as outlined in Section 1.4:

$$E_k \approx \frac{1}{2} m \langle v_z^2 \rangle = \chi E_L - E_a, \quad (13)$$

where  $E_a$  is a term representing a threshold energy deposition required for significant ablation, and  $\chi$  is the usual transmission term accounting for plasma and reflectivity effects. For strict theoretical consideration,  $E_a$  should be based on the threshold energy density in the target necessary for degradation. Thus, in the form of energy,  $E_a$ , the threshold term also implicitly carries a dependence on the characteristic ablated volume, which may be approximated as the product of the laser spot area and the threshold depth. In terms of the content of  $E_a$ , the threshold includes energetic modes (*e.g.*, thermal, rotational, vibrational, or electronic), as well as factors such as the latent heat of vaporization, and for polymer targets, energy necessary to break bonds linking monomer units. For either photochemical or photothermal ablation,  $E_a$  should also include the energy which is lost by radiation, and the energy which heats but does not ablate other portions of the target (for instance by transmission beyond the ablated area, or by thermal diffusion). In practice, it is feasible to represent all of these effects with a single, effectively constant term  $E_a$ ; however, the threshold is also dependent on parameters like the fluence [69].

Furthermore, the plume does not exhibit perfectly one-dimensional flow from the surface. Two- and three-dimensional effects, usually considered together as ‘plume divergence’, tend to reduce the total imparted impulse. Characterization of plasma regime ablation plumes performed by Kelly and Dreyfus [87] suggests that the yield (*i.e.*, ablated particle number density) at a particular angle  $\theta_{ex}$  from the surface normal is related to  $(\cos \theta_{ex})$  raised to some power. For vaporization, an analogous condition probably holds; however, the form of such a function is unknown to the authors, so we will assume that the effective distribution is a product of  $\langle v_z^2 \rangle$  and an analytical function  $\Pi$  that expresses the net

directionality of the exhaust, and which may depend on, among other things, the ambient pressure and the fluence, with limits:

$$\Pi = \begin{cases} \frac{1}{2}, & \text{hemispherically symmetric} \\ 1, & \text{uniaxial} \end{cases}, \quad (14)$$

representing ideal, uniformly three-dimensional and two-dimensional exhaust cases, respectively. We would expect uniaxial conditions to dominate when the spot area is large compared to the ablated depth, and the hemispherically symmetric conditions to represent a “worst case” performance. In practice,  $\Pi$  should be between these extremes.

The areal impulse density  $\sigma$  (impulse divided by ablated spot area) may be formed as the product of  $\mu$  and  $v_{\text{ex}}$ , which implicitly includes the directionality factor  $\Pi$ . For photochemical ablation, this is:

$$\sigma \approx \mu v_{\text{ex}} \approx \mu \sqrt{\Pi \langle v_z^2 \rangle} = \sqrt{\frac{2\rho\Pi}{\alpha} (\chi\Phi_L - \Phi_a) \ln \frac{\chi\Phi_L}{\Phi_a}}. \quad (15)$$

We will now turn to a discussion of two engineering parameters often used to characterize laser ablation propulsion. The momentum coupling coefficient

$$C_m = \sigma/\Phi \quad (16)$$

is also the ratio of imparted impulse to the laser pulse energy. It describes the effectiveness of thrust-production of a laser propulsion system. The specific impulse

$$I_{\text{sp}} = \sigma/(\mu g) \quad (17)$$

is also the imparted impulse divided by the product of the mass of used propellant and  $g = 9.8 \text{ m/s}^2$ . Although  $g$  is present in the expression for  $I_{\text{sp}}$ , it does not have any physical implications. For instance, the definition of  $I_{\text{sp}}$  is the same when used to describe electric propulsion thrusters on spacecraft, which only operate in microgravity.

Taking  $\Lambda = \chi\Phi/\Phi_a$ , Equation (15) yields the following photochemical  $C_m$  and  $I_{\text{sp}}$  expressions:

$$C_m = \sqrt{\frac{2\rho\Pi\chi^2}{\alpha\Phi_a} \frac{\Lambda-1}{\Lambda^2} \ln \Lambda} \quad \text{and} \quad I_{\text{sp}} = \sqrt{\frac{2\alpha\Phi_a\Pi}{\rho g^2} \frac{\Lambda-1}{\ln \Lambda}}. \quad (18)$$

These expressions are convenient for description of impulse within the photochemical regime; the relationships should be valid as long as photochemical vaporization is the primary ablation mechanism. The model will not be valid in regimes where ablation is dominated by other processes. For POM, based on analysis of thermal data from the literature presented above, some examples of other mechanisms include offgassing (at low temperatures), atomization, combustion, and plasma formation. Similar formulations of models for photothermal ablation can be expressed:

$$C_m = 2\chi \left( \frac{\Psi^2 D\tau\rho^2}{\Phi_a^2} \right)^{1/4} (\ln \Lambda)^{1/4} \sqrt{\frac{\Lambda-1}{\Lambda^2}} \quad \text{and} \quad I_{\text{sp}} = \sqrt{\frac{\Phi_a\Pi}{\rho g^2 \sqrt{D\tau}} \frac{\Lambda-1}{\sqrt{\ln \Lambda}}}. \quad (19)$$

Phipps, *et al.* [64] derived an impulse generation model for use in the plasma regime for  $C_m$ ;  $I_{\text{sp}}$  is also expressible, using the results given in [64]:

$$C_m = (1.84 \times 10^{-4}) \frac{\Psi^{9/16} \tau^{1/8}}{A^{1/8} \Phi^{1/4} \lambda^{1/4}} \cdot \text{and} \quad I_{sp} = (4.42 \times 10^2) \frac{A^{1/8} \Phi^{1/4} \lambda^{1/4}}{\Psi^{9/16} \tau^{1/8}} \cdot \quad (19)$$

Reference 65 combined the above results with the vaporization model of References 22 and 63 using a semi-empirical interpolation formula relying on the ionization ratio  $\beta$  (*i.e.*, ignoring effects at moderate ionization ratios) to provide a linear bridge from the vaporization regime to the highly-ionized plasma regime:

$$\sigma \approx \beta \sigma_{\text{plasma}} + (1 - \beta) \sigma_{\text{vaporization}} \cdot \quad (20)$$

The expected result is shown in Figure 9:

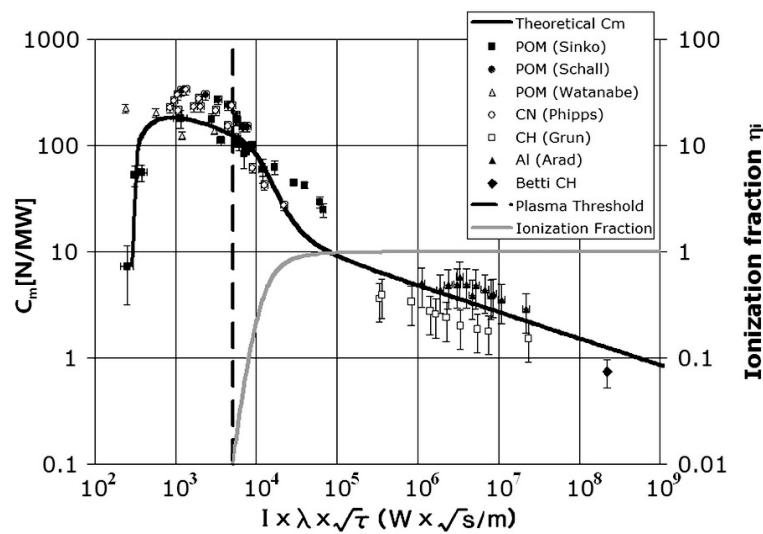


Figure 9. Vaporization to the plasma regime (Reprinted with permission from J. E. Sinko and C. R. Phipps, “Modeling CO<sub>2</sub> laser ablation impulse of polymers in vapor and plasma regimes, *Applied Physics Letters*, **95**(13), 131105 (2009). Copyright 2009, American Institute of Physics.)

This broad description of laser ablation covers photochemical impulse generation from vaporization into the plasma regime, and can be applied to analysis of both  $C_m$  and  $I_{sp}$ . Taken together, the above expressions can describe most of the CO<sub>2</sub> laser ablation studies on POM that were reported in the literature.

Another interesting feature of  $C_m$  is worthy of note. Plotting (18) above as a function of  $\Phi$  (or  $\Lambda$ ), one quickly discovers that the predicted curve grows, reaches a maximum value  $C_{m, \text{opt}}$  at a fluence  $\Phi_{\text{opt}}$ , then asymptotically decreases as  $\Phi$  continues to rise, as illustrated in Figure 9. The optimal fluence  $\Phi_{\text{opt}}$  was categorized by Gregg and Thomas [88], and indicates the fluence level at which the maximum  $C_m$  is achieved for a given laser beam and target material. This behavior has been conclusively established by experimental studies by countless studies, although there is an ongoing debate about whether its origin is related to plasma attenuation, or merely to vaporization processes. We may also note that the optimum coupling is not always optimal for a given propulsion application. Similar peaks in  $C_m$  curves have been found in ablation studies using polymer, liquid, and even metal targets (for an interesting analysis of such experimental work, see, *e.g.*, References 53 and 64). Maximum coupling is obviously desirable from a laser propulsion standpoint, so a model that predicts this value should aid in the selection of efficient laser ablation target materials.

Interest in the fluence-dependent behavior of laser propulsion parameters is not limited to  $C_m$  - studies have also investigated mass removal, specific impulse, *etc.* Many literature studies have made

some account of fluence dependence; hence, there is a healthy body of literature data available for use. Any comprehensive treatment of fluence-dependence in laser impulse generation must account for several experimentally demonstrated features including  $\Phi_a$ , the critical threshold for plasma formation  $\Phi_p$  (based on  $n_{cc}$ ), and  $\Phi_{opt}$ . Other parameters, such as  $\mu$  and  $I_{sp}$ , are also important for the laser propulsion applications, and are discussed below.

Estimation of a laboratory ablation threshold  $\Phi_a$  (for our purposes here, the threshold could be either thermal or optical) is complicated by the difficulties in measuring fluence accurately for high-energy pulsed CO<sub>2</sub> lasers. Some variation in the value is expected between groups due to differences in laser systems and measurement techniques, but values reported in the literature range from about  $2 \times 10^3$  J/m<sup>2</sup> [7] to  $1.3 \times 10^4$  J/m<sup>2</sup> [15,22]. Exactly which photochemical and/or photothermal processes are represented by this initial threshold are not entirely clear; however, the primary threshold in fluence is probably associated with the energy deposition required to significantly degrade POM into CH<sub>2</sub>O monomer units. It is likely that several smaller thresholds would also be uncovered by careful, dense data collection representing initial polymer bond breaking and subsequent steps in the breakup of the formaldehyde units. It is also unclear whether  $\Phi_a$  has any dependence on the spot area or the ambient pressure.

In principle, the value of  $\Phi_{opt}$  may be affected by other considerations such as shot number and target geometry, but if such extraneous considerations are neglected, some interesting relationships can be derived. Maximizing the vaporization-based analytical  $C_m$  model of Equation (18) in terms of  $\Phi$ , one may solve a transcendental equation to find an analytical expression for the optimum fluence. Using  $A_{opt} = \Phi_{opt}/\Phi_a$ , the solution is  $A_{opt} \approx 4.2$ , as reported by Sinko and Gregory [22,63]. The solution should apply to photochemical ablation in vacuum, and is not restricted to ablation using a CO<sub>2</sub> laser, or to a POM target. For comparison, a similar, semi-empirical vaporization model was previously proposed by Phipps [64]:

$$C_m \approx C \sqrt{\frac{\rho}{c_p}} \sqrt{\Lambda} \sqrt{1 - \frac{1}{\Lambda} - \frac{\ln \Lambda}{\Lambda}} \approx C \sqrt{\frac{\rho}{c_p}} \frac{\sqrt{\ln \Lambda}}{\Lambda} (\sqrt{\Lambda - 1} - 1), \quad (21)$$

where  $C$  is an experimental constant particular to the laser-material combination and  $\Lambda = \alpha \Phi / c_p$  (implying  $\Phi_a = c_p / \alpha$ ). Equation (21) was maximized to find a corresponding optimum value [65]:  $A_{opt} \approx 6.9$ . As with the previous model, this result should be valid in vacuum for photochemical ablation.

Taking  $\Phi_a \approx 1.3 \times 10^4$  J/m<sup>2</sup> [22], one expects the optimum fluence at  $\Phi_{opt} \approx 9.0 \times 10^4$  J/m<sup>2</sup> for the Phipps model or  $\Phi_{opt} \approx 5.5 \times 10^4$  J/m<sup>2</sup> for the Sinko model. Although some results [15,22] are consistent with these predictions, most literature reports [4,14,21], made in air and vacuum, place  $\Phi_{opt} \sim 2 \times 10^5$  J/m<sup>2</sup>, significantly higher than predicted by either model. It may be noted that groups reporting high values for  $\Phi_{opt}$  were generally using laser systems with longer pulses, and operating at higher pulse energies, in some cases with a nozzle coupled to the target. In some studies made in air, significant combustion was also found. It is therefore impossible at the present time to categorically validate or invalidate the model predictions. The discrepancy could arise, for instance, from thermal diffusion, combustion, plasma attenuation, or confinement. Such effects were not included in the models, and their presence certainly could influence  $\Phi_{opt}$ . These effects deserve careful, more detailed study. A precise determination of the threshold fluence as well as the optimal coupling is necessary to properly test the models. The parameters  $a$  and  $P_0$  should be held constant in any such test.

Fluence-dependent literature results for ablated mass are shown in Figure 10 for low- and atmospheric-pressure conditions, with the ablated mass expressed as the areal mass density  $\mu$ .

There appears to be a trend towards higher mass removal as fluence increases until about  $2-3 \times 10^5$  J/m<sup>2</sup>. Reduced mass removal, particularly above about  $3 \times 10^5$  J/m<sup>2</sup> in air, can be attributed with some certainty to the presence of absorbing plasma above the material surface. However, note that at least some data values in air with fluence as high as  $10^6$  J/m<sup>2</sup> still appear to follow the unattenuated trend, indicating that the critical limit for plasma attenuation is dependent on experimental conditions (e.g., surface condition of the target, heating effects, focal length and quality of lens used (which influences the fluence distribution within the Rayleigh range), and quality and composition of the ambient atmosphere). However, most measurements in air conform to the masked trend corresponding to reduced mass removal, and regardless,  $2 \times 10^5 - 1 \times 10^6$  J/m<sup>2</sup>, about 1 order of magnitude, remains a very

narrow range of fluence for the appearance of a critical effect like plasma electron number density. In vacuum conditions, the mass removal appears to continue to increase even above a laboratory fluence of  $10^6 \text{ J/m}^2$ , with little-to-no attenuation observed. This observation indicates first, that plasma is more readily triggered at high pressure conditions, and second, that ablation in space conditions where high  $I_{sp}$  is needed (i.e., under vacuum), is unimpeded by plasma effects. It is unclear if the plasma triggered at high pressure is composed of air, ablated material, or both.

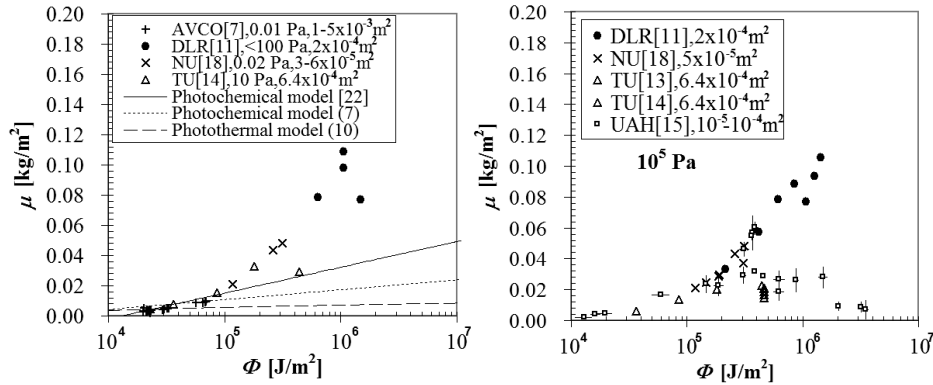


Figure 10.  $\mu(\Phi)$  for POM ablation at pressures <100 Pa (left) and 101 kPa (right)

In Figure 10, the unattenuated data trend significantly outruns the anticipated logarithmic trend in mass removal predicted by the photochemical model. The predictions of the photothermal model are even lower. Given the analysis of photochemical vs. photothermal effects presented earlier, this result is surprising. An improved mass-removal model is needed to explain the observed trends at high fluence. It is probable, for instance, that thermal effects become increasingly important with increasing plasma absorption. Radiation from the plasma at wavelengths other than 10.6 mm may be more strongly absorbed by the POM surface than the primary  $\text{CO}_2$  pulse; in fact, the trend in mass-removal appears to deviate from the photochemical prediction at about the same fluence as the critical plasma threshold. These effects could enhance mass removal from the surface during ablation by a secondary, thermal process. For instance, the data of Anju, *et al.* suggest that non-trivial thrust continues after the main force peak [17]. The described mass-removal trend applies to both vacuum and atmospheric conditions.

Another useful parameter is the ablated mass density per laser energy input,  $\xi = \mu / E_L$ , for which data is presented in Figure 11.

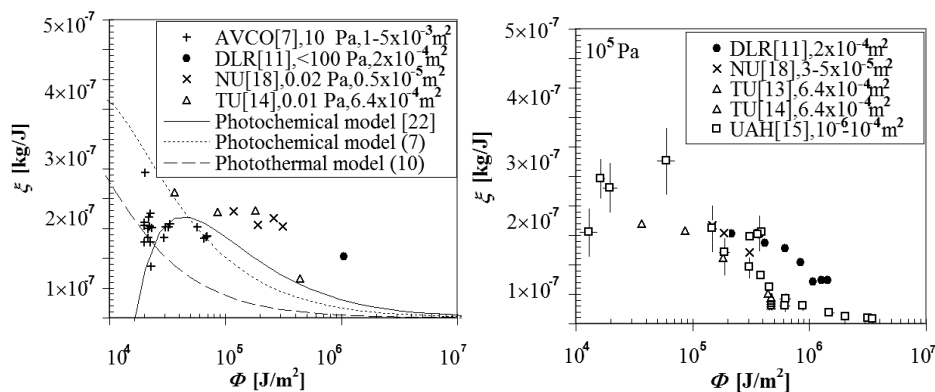


Figure 11.  $\xi(\Phi)$  for <100 Pa (left) and 101 kPa (right)

Results in Figure 11 are consistent with an increase to a peak  $\xi$  at a maximum of about 200-300 mg/J near the ablation threshold, followed by a decreasing trend until about  $2 \times 10^5 \text{ J/m}^2$ , and thereafter falling even more steeply above  $2\text{-}3 \times 10^5 \text{ J/m}^2$ , and finally falling to insignificance above  $\sim 5 \times 10^6 \text{ J/m}^2$ . The knee at  $2\text{-}3 \times 10^5 \text{ J/m}^2$  probably aligns with the onset of critical plasma effects and shielding. In light of

the data in Figure 10, it is interesting to note that in spite of an extraordinary increase in  $m$  above  $2 \times 10^5$  J/m<sup>2</sup>, the declining trend in  $\xi$  indicates that all increases in  $\mu$  are outweighed by energy costs.  $\xi$  provides an important counterpoint to  $\mu$  for consideration of mass removal. An improved  $\xi$  model is probably needed in this region.

The momentum coupling coefficient for POM is of great interest for laser propulsion applications. Values of  $C_m$  ranging from about 100-500  $\mu\text{Ns}/\text{J}$  have previously been reported in the literature. If the ambient pressure is high, the mechanical impedance of the ambient gas can enhance the impulse performance because the high-pressure region is confined for a longer time. Much of the reported data was enhanced even further using nozzles. For instance, enhancement of  $C_m$  for CO<sub>2</sub> laser ablation of POM up to at least a factor of five was demonstrated using nozzles [23] and other types of confinement [13,89,90]. The assembled literature data is shown in Figure 12. The data generally indicates a maximum coupling  $C_{\text{opt}}$  of around 200-300  $\mu\text{Ns}/\text{J}$  in vacuum and 150-250  $\mu\text{Ns}/\text{J}$  in atmospheric air. The model of Reference 22 can be used to predict the maximum value of the coupling coefficient (here we have neglected  $\mathcal{I}$ , for consistency with [22]). Using the in-air (in this case,  $\chi$ ,  $\alpha$ , and  $\Phi_a$  were fit by experiment) parameters of Reference 22,  $\rho \approx 1,430$  kg/m<sup>3</sup>,  $\chi^2 \approx 0.07 \pm 0.01$ ,  $\alpha \approx (1.9 \pm 0.2) \times 10^5$  m<sup>-1</sup>, and  $\Phi_a \approx (1.35 \pm 0.06) \times 10^4$  J/m<sup>2</sup>, and substituting  $A$  with maximal solution 4.244 in Eq. (18), we find:

$$C_{\text{opt}} = \sqrt{\frac{2\rho\chi^2}{\alpha\Phi_a} \frac{4.244-1}{4.244^2} \ln 4.244} \approx 140 \frac{\mu\text{Ns}}{\text{J}}, \quad (22)$$

which is slightly low compared to the vacuum data, but generally consistent with the literature results in air in Figure 12. Unfortunately, while the model of [22] conforms reasonably well to the data, it seems that the parameter fitting predicts physical values far from the physical values found in the literature. But if the representative physical values chosen in this paper:  $\chi = 0.9$ ,  $\rho \approx 1420$  kg/m<sup>3</sup>,  $\alpha \approx 1000$  cm<sup>-1</sup>, and  $\Phi_a \approx 2.5 \times 10^3$  J/m<sup>2</sup> are used instead, we find  $C_{\text{opt}} \approx 1500$   $\mu\text{Ns}/\text{J}$ , which is clearly inaccurate. For the photothermal model, again using representative values, we find  $C_{\text{opt}} \approx 530$   $\mu\text{Ns}/\text{J}$ , which is too high, even for vacuum data. In either case, the situation is improved, but not completely fixed, if  $\mathcal{I}$  is included. It follows that the existing models are simply not consistent with the data. Additional work is needed to sort out the reasons behind this discrepancy.

The  $C_m$  data above is also generally consistent with the reported ablation threshold fluences ( $0.2$ - $1.3 \times 10^4$  J/m<sup>2</sup>) [22]; however, more data is needed to confirm this value. Additionally, data from groups using laser systems with different operating characteristics could confirm effects from other parameters; *e.g.*, pulse shape and pulse length. As previously noted, there is some disagreement between reported values of  $\Phi_{\text{opt}}$ . The spread in existing data has prevented exact analysis, but the data seems to place  $\Phi_{\text{opt}}$  within the general range from about  $5 \times 10^4$ - $2 \times 10^5$  J/m<sup>2</sup>, as shown in Figure 12b. It is likely that  $\Phi_{\text{opt}}$  is strongly influenced by several control parameters, including, but not limited to, ambient pressure (*i.e.*, high  $P_0$ ) and confinement geometry (*e.g.*, nozzles). Thermal effects (*e.g.*, from long laser pulse lengths) are also likely to influence the position of  $\Phi_{\text{opt}}$ . Note that for  $C_m$  models (18) and (19), the peak occurs far outside the dataset, and it appears that the data, in fact, is inconsistent with both models, except at high fluence.

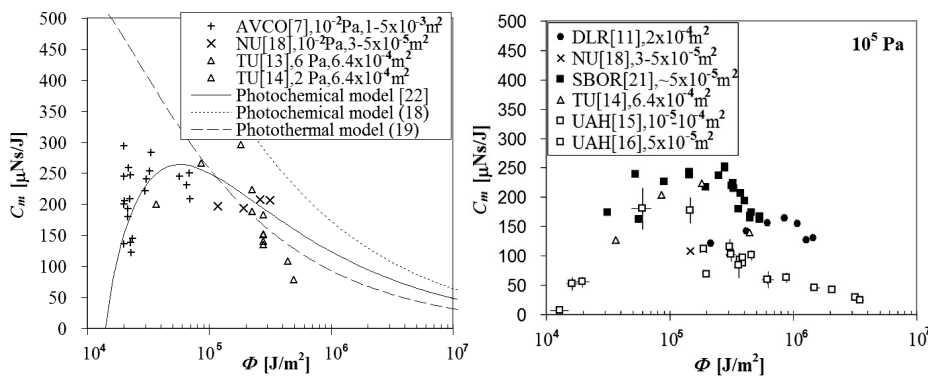


Figure 12.  $C_m(\Phi)$  for POM ablation at  $<100$  Pa (left) and at 101 kPa (right).

Specific impulse is in common use in propulsion science as a measure of propellant or fuel conservation. Reported literature results for  $I_{sp}$  are roughly consistent between air and vacuum conditions, as shown in Figure 13. The model fit to the data is not so good; the impulse overestimation at low fluence and mass underestimation at high fluence combine to push both models (18) and (19) higher than the literature data. Interestingly, there appears to be no significant change in the specific impulse trend as the plasma threshold is crossed.

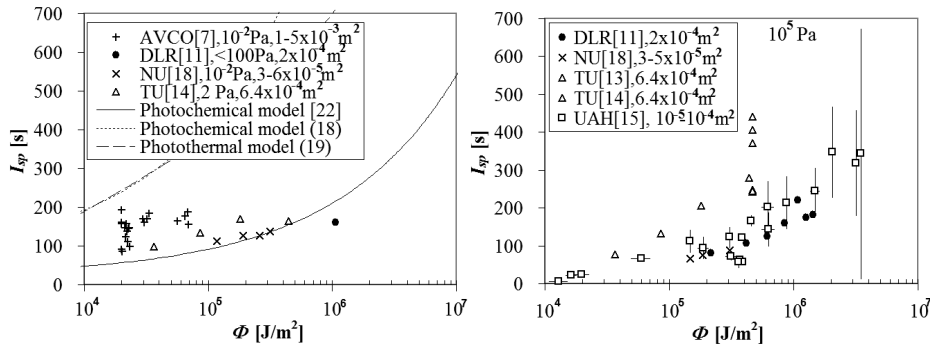


Figure 13.  $I_{sp}(\Phi)$  for ablation of POM at  $<100\text{ Pa}$  (left) and  $101\text{ kPa}$  (right)

The data in Figure 13 actually indicates a potential shortcoming of using POM for space applications. Unconfined ablation of POM in vacuum so far produced  $I_{sp} \sim 100\text{-}250\text{ s}$ . If ablation at higher fluence can be achieved without incurring plasma attenuation effects, this may not be a serious issue; however, the results indicate the probable necessity of some optics at the target for achieving high fluence, if this ablation mode is to be used in space. For atmospheric ablation, reasonable  $I_{sp}$  on bare propellant was only achieved at high fluence, where plasma shielding effects would dominate. Thus, in general, enhancement is *necessary* for significant impulse generation in an ablation environment at atmospheric pressure.

### 5.2 Ambient Pressure Dependence

Another topic for which there is some prior understanding is the dependence of propulsive performance on the ambient pressure. Ablation data in vacuum remains sparse in the laser ablation propulsion literature, particularly studies of ambient pressure dependence. Apart from some related work using different lasers or different target materials, to date, such study was performed almost exclusively by Watanabe [14] and Schall [10]. Some experimental data at low pressures was also reported by AVCO [7] and NU [18,20] and may be compared to the pressure-dependent studies. Data at  $10^5\text{ Pa}$  ambient atmosphere from SBOR [21] and UAH is also provided for comparison at high pressure [16]. The existing data for  $\mu$ ,  $C_m$ ,  $I_{sp}$ , and  $\xi$  are shown below in Figures 14-17.

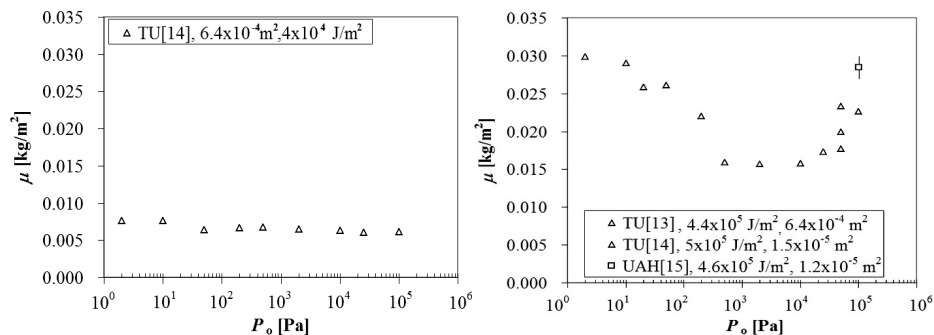


Figure 14.  $\mu(P_o)$ , low-fluence (left) and high-fluence (right)

The trend in mass removal apparently depends on the applied fluence. At low fluence,  $\mu$  appears to decrease slightly at high pressures. At high fluence, a depressed region of the curve is seen in the data from Watanabe [14]. This trend appears to be absent from the low-fluence data. Experimental data by other groups in these conditions is generally consistent with the results.

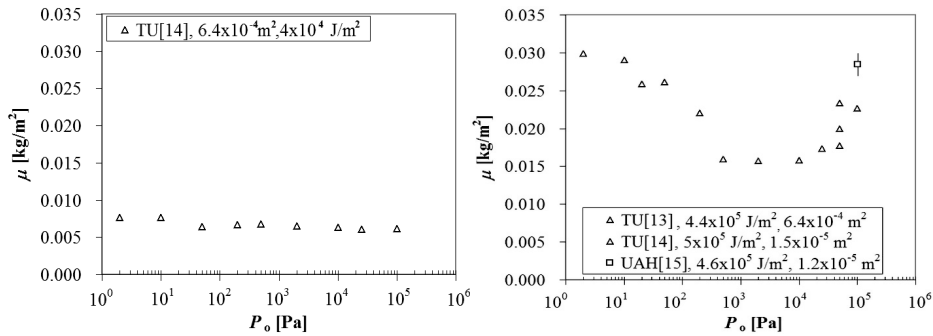


Figure 15.  $\xi(P_0)$ , low-fluence (left) and high-fluence (right)

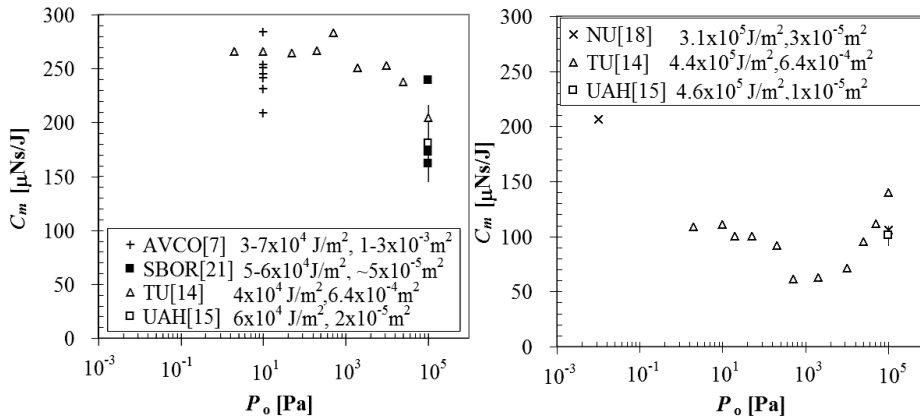


Figure 16.  $C_m(P_0)$ , low-fluence (left) and high-fluence (right)

The Watanabe  $C_m$  data appears to be confirmed by several other literature results, but a thorough independent check is advisable. The source of the dip at moderate pressures in  $C_m$ , at high fluence, is still not understood.

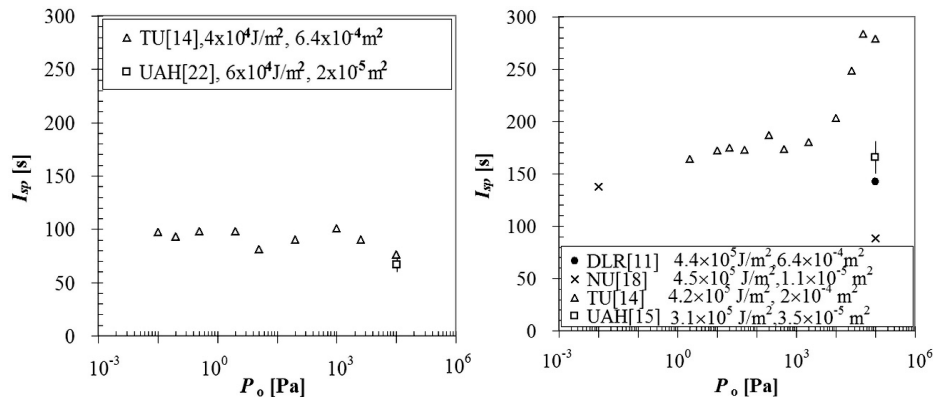


Figure 17.  $I_{sp}(P_0)$ , low-fluence (left) and high-fluence (right)

In Figure 17, the data of Watanabe [14] is curious due to the increase in  $I_{sp}$  at high fluence, with increasing ambient pressure. This trend is not supported by data taken in atmosphere at DLR, NU, and UAH, which exhibited roughly the same  $I_{sp}$  as in vacuum, about half the value found in the TU study. The source of the discrepancy is unclear. Because of the level of detail of the TU study, and the fact that the same trend was produced in several related experiments at TU with slightly different setup conditions, it is unlikely that the depressed region is an artifact (*e.g.*, from some form of systematic noise); nevertheless, it may be representative of peculiarities of the laser system, experimental setup, or measurement techniques. The trend from the Watanabe data set remains unexplained, and it is hoped that future research may clarify the physics underlying the results.

### 5.3 Spot Area Dependence

One important topic that has been largely ignored, perhaps due to its surprising complexity, is the dependence of laser ablation impulse on the laser spot area. This is important, for instance, in determining whether a larger size would be beneficial or detrimental to a vehicle design.

Based on geometry and scale sizes, we may argue that spot area effects would become significant only when the spot area is on the order of (or smaller than) the thickness of the ablation and acceleration layers. The ablated depth per pulse is typically on the order of 0.1-100 mm for CO<sub>2</sub> laser ablation of POM. Because the diffraction-limited spot size of CO<sub>2</sub> lasers is around 100 mm, such effects might not be seen in practice. However, there are also various effects that have scale sizes >100mm, such as redeposition and diffraction.

One possible contribution was revealed by fluid dynamics simulations of ablation exhaust [91] in which the geometric freedom provided at the edges of the ablation spot allowed additional mass to escape from the ablation area compared with the center of the spot. This resulted in relatively sharp crater edges with the maximum ablation at the edge instead of the center of the beam. So far, to the authors' knowledge, significant profilometry studies of CO<sub>2</sub>-ablated targets were not performed in the literature.

For real systems, pressure-dependence of impulse generation and self-confinement effects in the exhaust may improve this relationship somewhat, but the degree to which such effects actually enhance the impulse remains unclear. In addition, range issues will have to be considered, due to the divergence of the laser beam.

The influence of spot area effects from focusing the laser beam generally cannot be ignored for transparent targets, since the spot is smaller at the beam waist than at the surface. However, since the penetration depth of POM is only a few mm for CO<sub>2</sub> laser ablation, the most important parameter is the laser beam spot size at the surface.

Aerodynamic and hydrodynamic spot area effects were previously studied experimentally, theoretically, and numerically by Pirri [92], Reilly [93], and Zeifman [94]. However, the sparseness of data points prevents any detailed model development from their results. Furthermore, as the previous studies were developed generally for the plasma regime and metal targets, it is unlikely that they would be entirely applicable to CO<sub>2</sub> laser ablation of a polymer. In fact, to the authors' knowledge, so far the only significant experimental contributors to ablation area scaling of POM have been DLR [11], NU [18] and UAH [95-97]. Moreover, Nagoya University reported only a few data points on this subject, not enough to assemble a solid trend in performance. The DLR results are complicated by the radial ablation geometry and nozzle confinement. The UAH data, possibly the most complete picture so far, did not cover a wide enough range of area to be meaningful. Measurements made using different equipment and different conditions were compared. In addition, some of the reported trends in vapor plume heights may have resulted from limitations of the imaging system, rather than ablation phenomena. An initial comparison of the UAH data against some different groups' data from  $\Phi \approx 3 \times 10^5 - 4 \times 10^5$  J/m<sup>2</sup> and  $P_o \approx 101$  kPa is shown in Figure 18, and indicates that the previously reported experimental trends may be local area effects or experimental artifacts, since other existing data is relatively flat with increasing spot area.

At small spot sizes, the spot area dependence may be expected to be influenced by the position of the rarefaction wave during the ablation process, which propagates from the edges of the pressure disturbance towards the center, and may be expected to occur on a time scale of the laser pulse and following a sound speed on the order of that of the local environment. In atmospheric conditions the sound speed is around 340 m/s, and for a typical CO<sub>2</sub> laser with 5 ms pulse length, this yields a length scale (*i.e.* spot radius) on the order of 2 mm; *i.e.*,  $a \approx 9 \times 10^{-6}$  m<sup>2</sup>. Most of the UAH data in the above

figures is within the limits where such effects should be important. Of course, the sound speed of ‘hot’ ablation gas is much faster if it remains at high temperature over the laser spot. Although the length scale would be increased in that case, the rarefaction wave would also move more quickly, and it is unclear what net effect should be expected.

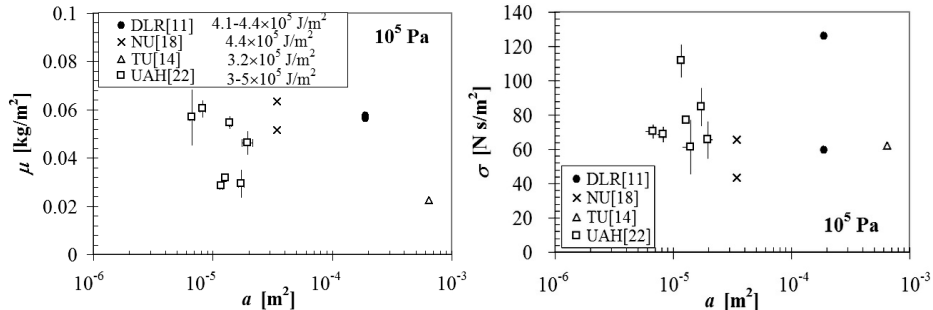


Figure 18.  $\mu a$  (left) and  $\sigma a$  (right) at atmospheric pressure

Another size scaling effect could arise from thermal diffusion, but in general, such effects in the lateral direction could only increase the spot radius by 1-10 mm. This size scale is less than the diffraction limited spot size for CO<sub>2</sub> lasers (~60 mm), as well as the wavelength of the radiation, and can be neglected in virtually any experimental configuration. However, the contribution to the ablated mass cannot always be neglected.

As a final note, the dramatic difference in the spot area geometry between stable and unstable oscillator configurations cannot be ignored, even for ablation on flat targets. This subject falls topically between spot area scaling effects and confinement effects. Unstable configurations were used at AFRL-PLVTS, DLR, Sosnovy-bor, and Tohoku University. Previous work at DLR (*e.g.*, see Reference 9) directly compared such geometries, finding some differences over the range of fluence tested for two different vehicle systems, but did not conclusively resolve the issue. The laser spot area dependence remains a critical issue for future investigation.

#### 5.4 Combustion and Confinement Effects

After fluence effects, the next best studied parameter space in the CO<sub>2</sub> laser ablation of materials is probably the set of combustion and confinement effects, because of the sheer volume of studies performed on vehicle systems utilizing confined CO<sub>2</sub> laser ablation of POM. However, while these impulse enhancement techniques are interesting, they are generally tangential to the chemical and physical issues of CO<sub>2</sub> laser ablation of POM on which this study is particularly focused. Therefore, a full treatment of these issues will not be made here. It is also important to note that separating combustion and confinement effects in atmospheric ablation of POM is very difficult, which is why the two effects are treated as two parts of one topic in this discussion. The scale size of combustion effects, which varies strongly with the interaction area (*i.e.*, the laser spot area) is often of the same order as confinement apparatus such as nozzles. However, the use of almost any nozzle should allow capture of additional impulse through increased interaction time between the exhaust and the confining target surface, regardless of whether combustion occurs.

Since air is made up of  $\approx 78\%$  N<sub>2</sub>, a good experimental test of combustion effects is between air and nitrogen atmosphere. This type of experiment was already conducted by at least three groups. At UAH, Sterling [16] addressed the confinement/combustion issue by testing POM ablation in nozzles, in air and inert (N<sub>2</sub>) atmospheres, finding enhancement of about 12% in air atmosphere compared to nitrogen. Work at DLR [10] using ‘Bohn Bell’-type parabolic nozzles found enhancement of about 16-20% for air atmosphere compared to N<sub>2</sub>. Finally, Ageichik, *et al.* [21] recently made a thorough analysis of energy from combustion of various CHO-type propellants, including POM. Experimental results demonstrated up to 30% impulse enhancement for ablation of POM in air compared to nitrogen atmosphere. Therefore, with use of a nozzle, combustion may be expected to add between 10-30% impulse enhancement compared to an inert atmosphere.

Studies focusing on some aspect of confined ablation have been made by practically every group which reported CO<sub>2</sub> laser ablation of POM. The studies include a bewildering variety of confinement

geometries, including conical [16,23,82], parabolic [10,71,72], cylindrical [11,13,21], and bi-parabolic nozzles [4,9], confining solid plates [13], confining liquid layers [90], and even in-tube ablation schemes [20]. It is also possible that results presented by Suzuki represent limited confinement by formation of a kind of nozzle in the ablation crater after many laser shots [18]. Typically these geometries result in enhancement of a factor of 2-10 over ablation of the bare propellant, but the relation of the geometries to specific dependencies such as pressure, fluence, and spot area is a formidably complex topic.

A final point of interest lies in whether extraordinary confinement effects are introduced by variation of the ablation geometry. For instance, vehicle concepts of the LJE [21,98] and 'Bohn Bell' [99] used radially incident laser radiation on a central propellant rod for ablation. Myrabo's study [4] used radial ablation of a ring. In each of these cases, the geometry might significantly influence ablation, for instance by self-focusing of an ablation plume by geometry, as opposed to by some external structure like a nozzle. Some confinement is probably necessary for cases of radial ablation, in order to redirect the otherwise laterally expanding exhaust into a useful, longitudinally directed exhaust plume.

### 5.5 Doping and Other Effects

In addition to consideration of homo- and co-polymer POM, various attempts have been made at doping POM to enhance its absorption, in the hopes of increasing the energy density in the exhausted propellant and therefore enhancing specific impulse. It may be mentioned at the outset that the bulk of the studies so far on doping of POM found little to no improvement in laser ablation propulsion performance. Early studies were conducted by AVCO [7] on custom Celcon<sup>®</sup> targets doped with silver-coated glass microspheres and separate targets doped with ~4% sodium valerate and aluminum flakes of about 2 mm thickness and 5mm diameter. Although greater energy deposition was found in air for the silver-coated microspheres, the results using aluminum flakes were suggestive that there was no improvement compared to plain Celcon<sup>®</sup>, despite testing in air, N<sub>2</sub>, and vacuum environmental conditions. Celcon<sup>®</sup> was reported to tolerate doping with metals much better than Delrin<sup>®</sup>. The improved resilience is probably related to its structure, described earlier. DLR [12] conducted a thorough study on targets of Delrin<sup>®</sup> loaded with 15-30mm-sized aluminum powder in 0%, 20%, 40%, and 60% concentrations, by weight. The powder increased absorption of the laser pulse by plasma before its arrival at the target surface, dramatically reducing the ablated mass at a concentration as low as 20%, but also dramatically reducing the imparted impulse. Granulation of the samples was observed by electron microscopy following ablation, indicating that the POM was being ablated while the metal flakes were left in the surface or ablated at a relatively low velocity. This process was universally associated with a reduction in performance compared to the undoped material. AFRL [82] and UAH [15,16] tested low-percentage (~0.2-1%) carbon-doped Delrin<sup>®</sup> samples; the commercially-doped material included a total of about 2-3% additives such as colorant, stabilizer, and antioxidant. In the UAH studies, the impulse measured for the carbon doped samples improved around 50% above undoped Delrin<sup>®</sup> during tests in atmosphere. However, the average results for the ablated mass density  $m$  of the doped and undoped targets were within 1%; *i.e.*, no significant change in the ablation depth was measured between the undoped and doped material. This result suggests that additional energy is absorbed into the exhaust of the doped material compared to the undoped polymer, although the mechanism is unclear.

Taken together, the results from the various doping studies suggest that large-percentage modification of POM by loading with absorbing materials does not increase performance. Absorption in POM is already relatively large compared to other polymers, so efforts to further increase absorption must be balanced against the expected effect on bulk material properties of the target. So far, efforts to dope or load POM have neglected this important consideration. Granulation effects during production, as well as during ablation, will seriously degrade performance by causing ejection of bulk material. Smaller-scale doping that has minimal effect on the material properties, such as in the samples studied by the AFRL and UAH, may hold some promise.

## 6. CONCLUSIONS AND RECOMMENDED WORKS

Data on CO<sub>2</sub> laser ablation of polyoxymethylene was assembled from literature sources and compared based on a variety of parameters related to laser propulsion performance. Effects from the experimental setup were considered, including measurement techniques, incident fluence, irradiated spot area, ambient pressure, confinement effects, combustion, surface conditioning effects, and solid solutions.

Fluence-dependence of laser ablation of POM is probably the most well-defined of the parameters simply because of the number of detailed studies; however, so far it has only been explored from about  $1 \times 10^4$ - $5 \times 10^6$  J/m<sup>2</sup>. The ablation threshold has been reported as  $2 \times 10^3$  and  $1.3 \times 10^4$  J/m<sup>2</sup>, and a sharp cutoff was noted in the literature data in the ablated mass and  $C_m$  data above about  $2 \times 10^5$ - $3 \times 10^5$  J/m<sup>2</sup>, which probably corresponds to a threshold for plasma formation. Values of  $\xi$  cut off rapidly above  $10^6$  J/m<sup>2</sup>.

Recently-proposed models for  $\mu$ ,  $C_m$ , and  $I_{sp}$  were fit to the literature data. The previous results were compared for the first time against thermodynamic data about vaporization conditions of POM. POM remains a good choice for a laser ablation propellant at a wide range of fluences. However, care must be taken in atmospheric conditions - especially in the range  $2 \times 10^5$ - $2 \times 10^6$  J/m<sup>2</sup> - to avoid operating in the plasma cutoff mode, which is associated with reduced ablated mass, reduced impulse, and generally decreased propulsion performance.

Pressure dependence was discussed, especially in light of plasma attenuation effects, combustion, and confinement. Existing data indicates a significant reduction in impulse at high pressures and moderate fluences, possibly associated with appearance of plasma attenuation effects. However, at high fluence, there may be a reversal of the trend.

Some initial studies on spot area effects were considered, with the conclusion that the data assembled so far is inadequate to appropriately treat this subject with the attention it deserves.

For the future, we note that CO<sub>2</sub> laser irradiation of POM is a good combination that can be used broadly for studying laser ablation propulsion. However, the specific impulse in reported works is unacceptably low (200 s or less). To gain merit via increasing payload fraction, laser propulsion research must still consider other materials capable of producing higher  $I_{sp}$  than that of chemical propulsion.

Additionally, the effect of ambient gas pressure is complex, and further diagnostic studies are needed to clarify these effects. Numerical studies of gas transport in the ablation plume - and of crater formation - are also needed in order to clarify the impulse generation mechanism. A related subject is the angular distribution of momentum flux in the ablation plume, possibly the most important parameter directly linked to impulse performance. Accurate measurement and understanding of the associated mechanisms are critical issues.

Finally, we believe it is time to discuss application of current laser propulsion knowledge to practical, fielded systems.

## ACKNOWLEDGEMENTS

The Micro-Nano Global Center of Excellence (GCOE) program and Nagoya University supported this study. A special measure of gratitude is extended to a number of individuals for their generous help in interpreting and analyzing previously published work on CO<sub>2</sub> laser ablation of polyoxymethylene, listed in alphabetical order by affiliation: Franklin B. Mead, Jr. and Carl W. "Bill" Larson (AFRL), Stefan Scharring and Hans-Albert Eckel (DLR), Stewart Millen, Kenneth Potts, Robert Sinko, and Jane Zhu (Eastman Chemical Company, Kingsport, TN), Yuri P. Rezunkov (Sosnovy-bor, Leningrad Region, Russia), Jordin Kare (Kare Technical Consulting, Seattle, WA, USA), Keiko Watanabe (OU), Claude Phipps (Photonic Associates, LLC, Santa Fe, NM, USA), David Rosen (Physical Sciences, Inc., Andover, MA, USA), Leik Myrabo (RPI), Stanislav I. Stoliarov (SRA International, Linwood, NJ, USA), Enrique Sterling (Trinity College, Ireland), Don A. Gregory (UAH), Andrew V. Pakhomov (formerly of UAH), and Clifford Schlecht (Washington University in St. Louis, St. Louis, MO, USA).

## REFERENCES

- [1] A. N. Pirri, R. Schlier, and D. Northam, Momentum transfer and plasma formation above a surface with a high-power CO<sub>2</sub> laser, *Appl. Phys. Lett.*, 21(3), 1972, 79-81.
- [2] F. B. Mead, Jr., L. N. Myrabo, and D. G. Messitt, *Flight and Ground Tests of a Laser-Boosted Vehicle*, AIAA Paper, 1998, 3735.
- [3] Air Force Research Laboratory, Lightcraft Researcher Honored by AIAA, *AFRL Propulsion Directorate Monthly Accomplishment Report*, Nov. 2001, 6-7.
- [4] L. N. Myrabo, M. A. Libeau, E. D. Meloney, and R. L. Bracken, *Pulsed Laser Propulsion Performance of 11-cm Parabolic 'Bell' Engines Within the Atmosphere*, AIAA Paper, 2002, 2732.
- [5] A. Butlerow, Ueber einige Derivate des Jodmethylen, *Liebigs Ann. der Chem* 111(2), 242-252 (1859), in German.

- [6] J. T. Kare, Program and Applications for a Near-Term Launch System, *Report*, Accession No. 4331, CA Report No. DE90011760, 1 Jun. 1989.
- [7] D.A.Reilly, Laser Propulsion Experiments - Final Report, *Final Report*, AVCO Research Lab, Inc., Everett, Maine 02149, Subcontract B116822 for University of California Livermore National Laboratory, Jordan Kare, Program Manager, 1991.
- [8] J. Kare, Laser Launch, the Second Wave, First International Symposium on Beamed Energy Propulsion, *AIP Conference Proceedings*, 664, 2003, 22-36.
- [9] W. O. Schall, W. L. Bohn, H.-A. Eckel, W. Mayerhofer, W. Riede, S. Walther, and E. Zeyfang, US German Lightcraft Impulse Measurements, *Final Report*, SPC00-4033, EOARD contract F61775-00-WE033, Apr. 2001, 1-47.
- [10] W. O. Schall, H.-A. Eckel, and S. Walther, Lightcraft Impulse Measurements under Vacuum, *Report*, SPC02-4017 EDOARD Contract FA8655-02-M4017, Sep. 2002, 1-64.
- [11] W. O. Schall, H.-A. Eckel, J. Tegel, F. Waiblinger, and S. Walther, Properties of Laser Ablation Products of Delrin with CO<sub>2</sub> Laser, *Final Report*, EOARD Grant, Cooperative Award No. FA8655-03-1-3061, May 2004.
- [12] W. O. Schall, J. Tegel, and H.-A. Eckel, Ablation Performance Experiments with Metal Seeded Polymers, Third International Symposium on Beamed Energy Propulsion, *AIP Conference Proceedings*, 766, 2005, 423-32.
- [13] K. Watanabe and A. Sasoh, Laser impulse generation required for space debris deorbiting, High-Power Laser Ablation V, *Proc. of SPIE*, 5448, 2004, 422-7.
- [14] K. Watanabe, K. Mori, and A. Sasoh, Ambient Pressure Dependence of Laser-Induced Impulse onto Polyacetal, *J. of Propulsion and Power*, 22(5), Sep.-Oct. 2006, 1150-3.
- [15] J. E. Sinko, A. V. Pakhomov, S. Millen, J. Zhu, R. J. Sinko, and K. Potts, Delrin® for propulsion with CO<sub>2</sub> laser: Carbon doping effects, Fifth International Symposium on Beamed Energy Propulsion, *AIP Conference Proceedings*, 997, 2008, 254-65.
- [16] E. Sterling, J. Lin, J. Sinko, L. Kodgis, S. Porter, A. V. Pakhomov, C. W. Larson, and F. B. Mead, Jr., Laser-Driven Mini-Thrusters, Fourth International Symposium on Beamed Energy Propulsion, *AIP Conf. Proc.*, 830, 2006, 247-58.
- [17] K. Anju, K. Sawada, A. Sasoh, K. Mori, and E. Zaretsky, Time-Resolved Measurements of Impulse Generation in Pulsed Laser-Ablative Propulsion, *J. of Propulsion and Power*, 24(2), Mar.-Apr. 2008, 322-9.
- [18] K. Suzuki, K. Sawada, R. Takaya, and A. Sasoh, Ablative Impulse Characteristics of Polyacetal with Repetitive CO<sub>2</sub> Laser Pulses, *J. Prop. & Power*, 24(4), Jul.-Auh. 2008, 834-41.
- [19] A. Sasoh, K. Mori, K. Anju, K. Suzuki, M. Shimono, and K. Sawada, *Time-Resolved and Integrated Laser Ablative Impulse Performance of Polyacetal*, AIAA Paper, 2007, 4389.
- [20] A. Sasoh, K. Mori, K. Anju, K. Suzuki, M. Shimono, K. Sawada, and E. Zaretsky, *Laser-Ablative Propulsion Using Polyacetal at Low Ambient Pressures*, AIAA Paper, 2007, 1185.
- [21] A. A. Ageichik, E. V. Repina, Y. A. Rezunkov, and A. L. Safronov, Detonation of CHO Working Substances in a Laser Jet Engine, *Technical Physics*, 54(3), 2009, 402-9. (translated from A. Ageichik, E. V. Repina, Y. A. Rezunkov, and A. L. Safronov, *Zhurnal Tekhnicheskoi Fiziki*, 2009, 76-83, in Russian)
- [22] J. E. Sinko, *Vaporization and Shock Wave Dynamics for Impulse Generation in Laser Propulsion*, Ph.D. Dissertation, The University of Alabama in Huntsville, Huntsville, AL, May 2008.
- [23] J. E. Sinko, N. B. Dhote, J. S. Lassiter, and D. A. Gregory, Conical nozzles for pulsed laser propulsion, High-Power Laser Ablation VII, *Proc. of SPIE*, 7005, 2008, 2Q, 1-10.
- [24] Yu. A. Rezunkov, A. L. Safronov, A. A. Ageichik, M. S. Egorov, V. V. Stepanov, V. S. Rachuk, V. Yu. Guterman, A. V. Ivanov, S. G. Rebrov, and A. N. Golikov, Performance Characteristics of Laser Propulsion Engine Operating both in CW and in Repetitively-Pulsed Modes, Fourth International Symposium on Beamed Energy Propulsion, *AIP Conference Proceedings*, 830, 2006, 3-13.
- [25] A. Haji-Sheikh, Y. S. Hong, S. M. You, and J. V. Beck, Sensitivity Analysis for Thermophysical Property Measurements Using the Periodic Method, *J. Heat Transfer*, 120, Aug. 1998, 568-76.

- [26] C. O. LaHoucine and A. Khellaf, Periodic Method: Correction for thermocouple and simultaneous estimation of thermal conductivity and thermal diffusivity, *Rev. Sci. Instr.*, 75(7), Jul. 2004, 2356-61.
- [27] K. N. Madhusoodanan, M. R. Thomas, and J. Philip, Photoacoustic measurements of the thermal conductivity of some bulk polymer samples, *J. Appl. Phys.*, 62(4), 15 Aug. 1987, 1162-6.
- [28] D. J. Holve, *Diffusion Controlled Combustion of Polymers*, Ph.D. Dissertation, The University of California, Berkeley, CA, 1974.
- [29] F. S. Dainton, D. M. Evans, F. E. Hoare, and T. P. Melia, Thermodynamic Functions of Linear High Polymers, Part I - Polyoxymethylene, *Polymer*, 3, 1962, 263-70.
- [30] R. C. Weast, ed., *CRC Handbook of Chemistry and Physics, 55th edition*, CRC Press, Cleveland, 1974, c-774.
- [31] M. Iguchi, Melting and Degradation Behaviour of Needle-like Poly(oxymethylene) Crystals, *Die Makromolekulare Chemie* 177, 1977, 549-66.
- [32] M. Inoue, Heat of Fusion and Interaction of Polyoxymethylene with Diluents, *J. Polymer Sci.*, 51(156), 1961, S18-S20.
- [33] M. Inoue, Studies on Crystallization of High Polymers by Differential Thermal Analysis, *J. Polymer Sci.: Part A*, 1, 1963, 2697-709.
- [34] H. W. Starkweather, Jr. and R. H. Boyd, The Entropy of Melting of Some Linear Polymers, *J. Phys. Chem.*, 64, 1960, 410-4.
- [35] H. W. Starkweather, Jr. and G. A. Jones, The Pressure-Volume-Temperature Relationship and the Heat of Fusion of Polyoxymethylene, *J. Poly. Sci.: Part B: Polymer Physics*, 26, 1988, 257-66.
- [36] H. Wilski, Die spezifische Wärme des Polyoxymethylens, *Kolloid-Zeitschrift & Zeitschrift für Polymere*, 248, 1-2, Oct. 1971, 867-70, in German.
- [37] R. E. Lyon and J. G. Quintiere, Criteria for piloted ignition of combustible solids, *Combustion and Flame*, 151, 2007, 551-9.
- [38] S. I. Stoliarov and R. N. Walters, Determination of the heats of gasification of polymers using differential scanning calorimetry, *Polymer Degradation and Stability*, 93, 2008, 422-7.
- [39] H. Suzuki, J. Grebowicz, and B. Wunderlich, Heat capacity of semicrystalline, linear poly(oxymethylene) and poly(oxyethylene), *Makromol. Chem.*, 186, 1985, 1109-19.
- [40] S. I. Anisimov and V. A. Khoklov, *Instabilities in Laser-Matter Interaction*, CRC Press, Boca Raton, 1995, Chapter 1: Interactions of Laser Radiation, 1.3 Laser-induced evaporation, 15-8.
- [41] T. Sukhanova, V. Bershtein, M. Keating, G. Matveeva, M. Vylegzhanina, V. Egorov, N. Peschanskaya, P. Yakushev, E. Flexman, S. Greulich, B. Sauer, and K. Schodt, Morphology and Properties of Poly(oxymethylene) Engineering Plastics, *Macromol. Symp.*, 214, 2004, 135-45.
- [42] M. Jaffe and B. Wunderlich, Melting of Polyoxymethylene, *Kolloid-Zeitschrift und Zeitschrift für Polymere*, 216-7, 1966, 203-16.
- [43] I. A. Abu-Isa, D. R. Cummings, D. E. LaDue, and A. Tewarson, *Thermal properties and flammability behavior of automotive polymers*, Factory Mutual Research Paper, 1998, S4-P-17, 911-9.
- [44] V. W. Kern and H. Cherdron, Der Abbau von Polyoxymethylenen: Polyoxymethylene. 14. Mitteilung, *Makromol. Chem.*, 40, 1960, 101-17, in German.
- [45] W. Kern, H. Cherdron, V. Jaacks, H. Baader, H. Deibig, A. Giefer, L. Höhr, and A. Wildenau, Polyoxymethylene, *Angewandte Chemie*, 73(6), 1961, 177-86, in German.
- [46] Y. Duan, H. Li, L. Ye, and X. Liu, Study on the Thermal Degradation of Polyoxymethylene by Thermogravimetry-Fourier Transform Infrared Spectroscopy (TG-FTIR), *J. Appl. Polymer Sci.*, 99, 2006, 3085-92.
- [47] M. W. Sigrest and Z. H. Chen, Analysis of Liquid Surface Films by Pulsed Laser Photoacoustic Spectroscopy, *Appl. Phys. B*, 43, 1987, 1-7.
- [48] S. A. Beckel and R. D. Matthews, Ignition of Polyoxymethylene, *Combustion and Flame*, 57, 1984, 71-86.
- [49] S. A. Beckel, *An Experimental Investigation of Synthetic Polymer Ignition*, M.S. Thesis, The University of Texas at Austin, Austin, TX, Aug. 1983.

- [50] P. Andre, Composition and thermodynamic properties of ablated vapours of PMMA, PA6-6, PETP, POM and PE, *J. Phys. D: Appl. Phys.*, 29, 1996, 1963-72.
- [51] Y. Tanaka, N. Yamachi, S. Matsumoto, S. Kaneko, S. Okabe, and M. Shibuya, Thermodynamic and Transport Properties of CO<sub>2</sub>, CO<sub>2</sub>-O<sub>2</sub>, and CO<sub>2</sub>-H<sub>2</sub> Mixtures at Temperatures of 300 to 30,000 K and Pressures of 0.1 to 10 MPa, *Elec. Eng. in Japan*, 163(4), 2008, 18-29. (translated from *Denki Gakkai Ronbunshi*, 126-B(1), 2006, 80-90, in Japanese.)
- [52] D. Bäuerle, *Laser Processing and Chemistry, Third Edition*, Springer-Verlag, Berlin, 2000, Chapter 2.2: The Heat Equation, 20; Chapter 7.5: Pulsed-Laser Irradiation, 128-9; Chapter 11.6: Plasma Formation, 206-10; Chapter 12.5: The Threshold Fluence,  $f_{th}$ , 238; Chapter 12.6.5: Influence of an Ambient Atmosphere, 246-7.
- [53] C. R. Phipps, Jr., T. P. Turner, R. F. Harrison, G. W. York, W. Z. Osborne, G. K. Anderson, X. F. Corlis, L. C. Haynes, H. S. Steele, and K. C. Spinochi, Impulse coupling to targets in vacuum by KrF, HF, and CO<sub>2</sub> single-pulse lasers, *J. Appl. Phys.*, 64(3), 1988, 1083-96.
- [54] M. Born and E. Wolf, *Principles of Optics, Seventh (Expanded) Edition*, Cambridge University Press, Cambridge, 1999, Chapter 1.5.2: Fresnel Formulae, 40-3; and Chapter 4.8.1: Basic Concepts of Radiometry, 194-9.
- [55] A. Cooke, Infrared Spectra of Polyoxymethylene Grains, *Astrophysics and Space Science*, 39(1), 1976, L13-L18.
- [56] H. Tadokoro, M. Kobayashi, Y. Kawaguchi, A. Kobayashi, and S. Murahashi, Normal Vibrations of the Polymer Molecules of Helical Configuration. III. Polyoxymethylene and Polyoxymethylene-*d*<sub>2</sub>, *J. Chem. Phys.*, 38(3), 1963, 703-21.
- [57] D. C. B. Whittet, I. J. Dayawansa, P. M. Dickinson, J. P. Marsden, and B. Thomas, The Optical Constants of Polyoxymethylene, *Mon. Not. R. Astr. Soc.*, 175, 1976, 197-207.
- [58] W. O. Schall, H.-A. Eckel, J. Tegel, and F. Holzschuh, Characterization of the Absorption Wave Produced by CO<sub>2</sub> Laser Ablation of a Solid Propellant, *Final Report*, EOARD Grant FA8655-04-1-3067, Oct. 2005, 16-7.
- [59] H. S. Carslaw and J. C. Jaeger, *Conduction of Heat in Solids, Second Edition*, Oxford University Press, Clarendon, 1959, Chapter 2.4, 75.
- [60] J. F. Ready, *Effects of High-Power Laser Radiation*, Academic Press, New York, 1971, Chapter 3, Absorption of Laser Radiation at Opaque Surfaces, D. Laser-Produced Vaporization, 100-6.
- [61] P. W. Milonni and J. H. Eberly, *Lasers*, John Wiley & Sons, New York, 1988, Chapter 13.9: CO<sub>2</sub> Electric-Discharge Lasers, 437-9.
- [62] S. Lee, CO<sub>2</sub> Processing at 9 microns, *Industrial Laser Solutions*, Mar. 1, 2002.
- [63] J. E. Sinko and D. A. Gregory, Critical fluence effects in laser propulsion, High-Power Laser Ablation VII, *Proc. of SPIE*, 7005, 2008, 1Z, 1-11.
- [64] C. R. Phipps, Jr., R. F. Harrison, T. Shimada, G. W. York, T. P. Turner, X. F. Corlis, H. S. Steele, L. C. Haynes, and T. R. King, Enhanced vacuum laser-impulse coupling by volume absorption at infrared wavelengths, *Laser and Particle Beams*, 8(1-2), 1990, 281-98.
- [65] J. E. Sinko and C. R. Phipps, Modeling CO<sub>2</sub> Laser Ablation Impulse of Polymers in Vapor and Plasma Regimes, *App. Phys. Lett.* 95(13), 2009, 131105.
- [66] J. E. Stewart, *Infrared Spectroscopy: Experimental Methods and Techniques*, Marcel Dekker, Inc., New York, 1970, Chapter 3: Superposition, Attenuation, and Reflection of Electromagnetic Waves, 82.
- [67] P. Hu, T. Shang, M. Jiang, and M. Chen, Investigation of the Thermal Decomposition Properties of Polyoxymethylene, *J. of Wuhan Univ. of Technology-Mater. Sci. Ed.*, 22(1), February 2007, 171-3.
- [68] V. Srinivisan, M. A. Smrtic, and S. V. Babu, Excimer laser etching of polymers, *J. Appl. Phys.*, 59(11), 1986, 38617.
- [69] N. B. Dahotre, ed., *Lasers in Surface Engineering*, ASM International, Ontario, 1998, Chapter 8, Lasers for Polymeric Coatings, P. P. Patil and M. A. More, 296-7; Chapter 2, Laser Surface Texturing, V. V. Semak and N. B. Dahotre, 46.

- [70] S. D. Knecht, C. W. Larson, and F. B. Mead, Jr., Comparison of Ablation Performance in Laser Lightcraft and Standardized Mini-thruster (Briefing Charts, POSTPRINT), Briefing Charts, *AFRL Report*, AFRL-PR-ED-VG-2005-393, 18 May 2005.
- [71] S. Scharring, H.-A. Eckel, and H.-P. Röser, Flight Analysis of a Parabolic Lightcraft - Ground-based Launch, Fifth International Symposium on Beamed Energy Propulsion, *AIP Conference Proceedings*, 997, 2008, 304-15.
- [72] S. Scharring, D. Hoffmann, H.-A. Eckel, and H.-P. Röser, Stabilization and steering of a parabolic laser thermal thruster with an ignition device, *Acta Astronautica*, 65(11-12), December 2009, 1599-615.
- [73] Private communication with Yuri P. Rezunkov, 2009.
- [74] Lumonics, Inc., *Instruction Manual: Lumonics® Series TEA-100-2 CO<sub>2</sub> Laser*, Oct. 1988, Series 100 Customer Test Report, 5.
- [75] H. Niino, T. Ohana, A. Ouchi, and A. Yabe, Polymer Ablation Upon Exposure to Vacuum Ultra-Violet Light, *J. Photopolymer Sci. and Tech.*, 5(2), 1992, 301-6.
- [76] H. Cottin, M.-C. Gazeau, J.-F. Doussin, and F. Raulin, An experimental study of the photodegradation of polyoxymethylene at 122, 147, and 193 nm, *J. of Photochemistry and Photobiology A: Chemistry*, 135, 2000, 53-64.
- [77] S. Torikai, Main-Chain Degradation and Thermal Stabilization of Polyoxymethylene by Ionizing Radiation, *J. Poly. Sci. A*, 2, 1964, 239-52.
- [78] E. Grossman and I. Gouzman, Space environment effects on polymers in low earth orbit, *Nuclear Instruments and Methods in Physics Research B*, 208, 2003, 48-57.
- [79] J. E. Sinko, C. R. Phipps, Y. Tsukiyama, N. Ogita, A. Sasoh, N. Umehara, and D. A. Gregory, *Critical Fluences and Modeling of Polyoxymethylene from Vaporization to the Plasma Regime*, Sixth International Symposium on Beamed Energy Propulsion, 1-5 November 2009, Scottsdale, AZ, USA, AIP Conference Proceedings, American Institute of Physics, In Press.
- [80] J. Sinko, *Time-Resolved Force and Imaging Measurement of the Laser Ablation of Liquids*, M.S. Thesis, The University of Alabama in Huntsville, Huntsville, AL, Dec. 2005.
- [81] J. S. Harchanko, F. B. Mead, Jr., and C. W. Larson, Impulse Pendulum with Adjustable Pivot Point for Measuring Coupling Coefficient, *AFRL Report*, Accession number ADA428438, Oct. 2004.
- [82] S. D. Knecht, C. W. Larson, and F. B. Mead, Jr., Comparison of Ablation Performance in Laser Lightcraft and Standardized Mini-thruster, Fourth International Symposium on Beamed Energy Propulsion, *AIP Conference Proceedings* 830, 2006, 615-627.
- [83] B. C. D'Souza and A. D. Ketsdever, Investigation of Time-Dependent Forces on a Nano-Newton-Second Impulse Balance, *Rev. of Sci. Instruments*, 76, 2005, 015105, 1-10.
- [84] J. E. Sinko and J. S. Lassiter, Sphere-Wall Impact Experiments with Piezoelectric Force Sensors, Fifth International Symposium on Beamed Energy Propulsion, *AIP Conference Proceedings* 997, 2008, 131-42.
- [85] V. M. Kuz'michev, B. V. Safronov, S. V. Pogorelov, and V. P. Balkashin, Measurement of the micrometer diameters of focused laser-beam radiation with a thin-wire bolometer, *Measurement Techniques*, 45(3), 2002, 264-7.
- [86] L. N. Myrabo, private communication, 9/9/2009.
- [87] D. W. Gregg and S. J. Thomas, Momentum Transfer Produced by Focused Laser Giant Pulses, *J. App. Phys.*, 37(7), 1966, 2787-9.
- [88] R. Kelly and R. W. Dreyfus, Reconsidering the Mechanisms of Laser Sputtering with Knudsen-Layer Formation Taken into Account, *Nuclear Instruments and Methods in Physics Research B*, 32, 1988, 341-8.
- [89] A. Sasoh, S. Suzuki, and A. Matsuda, Wall-ablative, laser-drive in-tube accelerator, High-Power Laser Ablation VII, *Proc. of SPIE* 7005, 2008, 0Z, 1-8.
- [90] J. E. Sinko, N. B. Dhote, and A. V. Pakhomov, Laser Propulsion with Liquid Propellants Part II: Thin Films, Fifth International Symposium on Beamed Energy Propulsion, *AIP Conference Proceedings* 997, 2008, 209-21.

- [91] T. Sakai, K. Ichihashi, A. Matsuda, and A. Sasoh, *Calculation of Pulsed Laser-Ablative Impulse on Polyacetal*, AIAA Paper, 2009, 3590.
- [92] A. N. Pirri, Theory for momentum transfer to a surface with a high-power laser, *The Phys. of Fluids*, 16(9), 1973, 1435-40.
- [93] J. P. Reilly, A. Ballantyne, and J. A. Woodroffe, Modeling of Momentum Transfer to a Surface by Laser-Supported Absorption Waves, *AIAA Journal*, 17(10), 1978, 1098-105. (presented as AIAA Paper, 1978, 177R).
- [94] M. I. Zeifman, B. J. Garrison, and L. V. Zhigilei, *Evolution of a Plume in Laser Ablation: Dependence on the Spot Size*, AIAA Paper, 2003, 3493.
- [95] J. E. Sinko, Constant-Fluence Area Scaling for Laser Propulsion, Fifth International Symposium on Beamed Energy Propulsion, *AIP Conference Proceedings* 997, 2008, 242-53.
- [96] J. E. Sinko, Measurements of shock waves produced by TEA CO<sub>2</sub> laser ablation in atmospheric conditions, *Symposium on Shock Waves in Japan*, proceedings published by Nagoya University, Nagoya, Japan, 2009, 291-2.
- [97] J. E. Sinko, Shock wave and vapor plume measurements for area scaling in laser propulsion, *Symposium on Shock Waves in Japan*, proceedings published by Nagoya University, Nagoya, Japan, 2009, 299-302.
- [98] A. A. Agechik, M. S. Egorov, and Yu. A. Rezunkov, The effect of aberrations on the focusing of laser radiation in a composite optical concentrator, *J. Opt. Technology*, 74(8), 2007, 563-68.
- [99] W. L. Bohn, Laser Lightcraft Performance, High-Power Laser Ablation II, *Proc. of SPIE*, 3885, 2000, 48-53.

